Using Advanced Very High Resolution Radiometer (AVHRR) satellite images to map snow cover and green biomass in Yellowstone National Park
by Donay Hanson

A thesis submitted in partial fulfillment of the requirements for the degree of Master of Science in Earth Sciences
Montana State University

Abstract:
Scientists and wildlife managers have expressed a desire for a method to identify areas of snow cover and green biomass concentration across regions such as Yellowstone National Park. Timing of snowmelt appears to drive the vegetation and ungulate population ecosystem in Yellowstone. The objective of this study was to produce an automated routine that processes Advanced Very High Resolution Radiometer (AVHRR) satellite images to produce snow cover and green biomass maps for non-forested areas of Yellowstone National Park. Although AVHRR has a low pixel resolution (1.1 km), daily images are available and are obtained easily. The advantage of using an automated method is that each daily image can be processed in the same manner, using a rigorously tested algorithm. Estimates of ground covered by snow (snow cover) from two aerial reconnaissance flights were regressed against raw and calibrated pixel numbers for the five band images from the corresponding days. The linear regression model using band 4 of georeferenced and calibrated AVHRR images estimated snow cover (Adjusted $R2 = 0.856$, $\alpha = 0.001$). To estimate green biomass, linear models derived by Thoma (1998) were used and ground reference data were collected during the growing season in Yellowstone National Park to evaluate the application of the model for this study area. Results of the linear model were satisfactory (Adjusted $R2 = 0.592$, $\alpha = 0.0001$). The algorithm is contained in a file created to aid in the use of the models for estimation of snow cover and green biomass. The file contains the Navigate program used to navigate and calibrate images, an Avenue script, containing the model for snow cover and green biomass estimation, the legend files for each legend, and a ReadMe with directions for using the algorithm, along with pertinent information concerning its limitations. The equations were implemented in an Avenue script for ArcView® to create maps of estimated snow cover (%) and green biomass (kg/ha) for Yellowstone National Park.

USING ADVANCED VERY HIGH RESOLUTION RADIOMETER (AVHRR) SATELLITE IMAGES TO MAP SNOW COVER AND GREEN BIOMASS IN YELLOWSTONE NATIONAL PARK

by

Donay Hanson

A thesis submitted in partial fulfillment
of the requirements for the degree

of

Master of Science

in

Earth Sciences

MONTANA STATE UNIVERSITY-BOZEMAN
Bozeman, Montana

December 2000

APPROVAL

of a thesis submitted by

Donay Hanson

This thesis has been read by each member of the thesis committee and has been found to be satisfactory regarding content, English usage, format, citations, bibliographic style, and consistency, and is ready for submission to the College of Graduate Studies.

Dr. Katherine Hansen	D. Katherine Hanson Co-Chairperson, Graduate Committee	11-28-00 Date
Dr. Rick Lawrence	Rick Lawrence Co-Chairperson, Graduate Committee	11/30/00 Date

Approved for the Department of Earth Sciences

Dr. James Schmitt	James A. Smith Head, Major Department	11-30-00 Date

Approved for the College of Graduate Studies

Dr. Bruce R. McLeod	Bruce R. McLeod Graduate Dean	11-30-00 Date

STATEMENT OF PERMISSION TO USE

In presenting this thesis in partial fulfillment of the requirements for a master's degree at Montana State University, I agree that the Library shall make it available to borrowers under rules of the Library.

If I have indicated my intention to copyright this thesis by including a copyright notice page, copying is allowable only for scholarly purposes, consistent with "fair use" as prescribed in the U.S. Copyright Law. Requests for permission for extended quotation from or reproduction of this thesis in whole or in parts may be granted only by the copyright holder.

Signature Dawn Hansen

Date November 30, 2000

ACKNOWLEDGEMENTS

First, I would like to thank my co-advisors, Dr. Katherine Hansen and Dr. Rick Lawrence, for their guidance on this thesis and negotiating graduate school. I appreciate Kathy's steadfast support, experience, and assistance with teaching assistantships. I value Rick's foresight in providing a lab equipped with state-of-the-art computers and an environment conducive to learning. The graduate students in the lab -- Shana Driscoll, Mark Fonstad, Mary Henry, Kathy Maynard, Linda Phillips, and Elizabeth Roberts, provided practical support and camaraderie during both easy times and crunch times. Dr. Richard Aspinall added to the feeling of camaraderie in the lab and provided assistance at critical times. Doug Chapman was a superb pilot and great fun to fly with. Thank you to those who understood when I could not participate in their lives during this process. This was a true lesson in what is important in life, especially where my young nephew was involved. Lianne Chong's sense of humor and understanding provided great inspiration to complete this thesis quickly during the final stages. Gillian's companionship was wonderful. Finally, a heartfelt 'thank you' to my parents, Patty Volker and Gene Hanson, for their financial support and words of wisdom, which made life bearable.

Financial support was partially provided by Upper Midwest Aerospace Consortium, Yellowstone National Park, and the Department of Earth Sciences, Montana State University.

TABLE OF CONTENTS

LIST OF TABLES

Table

LIST OF FIGURES

Figure

ABSTRACT

Scientists and wildlife managers have expressed a desire for a method to identify areas of snow cover and green biomass concentration across regions such as Yellowstone National Park. Timing of snowmelt appears to drive the vegetation and ungulate population ecosystem in Yellowstone. The objective of this study was to produce an automated routine that processes Advanced Very High Resolution Radiometer (AVHRR) satellite images to produce snow cover and green biomass maps for non-forested areas of Yellowstone National Park. Although AVHRR has a low pixel resolution (1.1 km), daily images are available and are obtained easily. The advantage of using an automated method is that each daily image can be processed in the same manner, using a rigorously tested algorithm. Estimates of ground covered by snow (snow cover) from two aerial reconnaissance flights were regressed against raw and calibrated pixel numbers for the five band images from the corresponding days. The linear regression model using band 4 of georeferenced and calibrated AVHRR images estimated snow cover (Adjusted R^2 = 0.856, $\alpha = 0.001$). To estimate green biomass, linear models derived by Thoma (1998) were used and ground reference data were collected during the growing season in Yellowstone National Park to evaluate the application of the model for this study area. Results of the linear model were satisfactory (Adjusted $R^2 = 0.592$, $\alpha = 0.0001$). The algorithm is contained in a file created to aid in the use of the models for estimation of snow cover and green biomass. The file contains the Navigate program used to navigate and calibrate images, an Avenue script, containing the model for snow cover and green biomass estimation, the legend files for each legend, and a ReadMe with directions for using the algorithm, along with pertinent information concerning its limitations. The equations were implemented in an Avenue script for ArcView® to create maps of estimated snow cover (%) and green biomass (kg/ha) for Yellowstone National Park.

CHAPTER 1

INTRODUCTION

The movement of wildlife in and out of Yellowstone National Park (the Park) is a primary concern to park managers (National Park Service 1998). Ungulates migrate along an elevation gradient, moving to lower elevations in the winter and following the green wave as snow melts and vegetation greens in the spring (Hobbs et al. 1981, Frank and McNaughton 1996, Merrill and Boyce 1996, Merrill et al. 1996, Singer 1996, Frank et al. 1998). Snow cover and green biomass maps are difficult to obtain in order to test this assumption on a regional scale. The need to understand ungulate migration is exacerbated because the Park's boundaries encompass the thermal features, rather than essential ungulate habitat. Ungulate populations therefore migrate to snow free areas across Park boundaries (Yellowstone National Park 1990, Yellowstone National Park 1997, Frank et al. 1998, National Park Service 1998). Management policies vary substantially among the National Park Service, other Federal agencies, and state agencies surrounding the Park, accounting for the need to have coordinated, multi-agency wildlife management strategies (National Park Service 1998).

Data on ungulate distribution are available to compare with snow cover and green biomass distribution. Aerial counts of elk (*Cervus elaphus*) on the northern range began in the early 1980s and counts of bighorn sheep (*Ovis canadensis*) extend back to the mid-1970s. Beginning in 1996, aerial counts of mule deer (*Odocoileus hemionus*) were conducted in December and in March with spring green up. A study of distribution was

conducted on pronghorn (*Antilocapra americana*) in the late 1980s. Data collection on bison (*Bison bison*) distribution began in the early 1960s (P. Gogan, personal communication). Due to the nature of these data, regional daily estimates of snow cover and green biomass were necessary. The ability to estimate snow cover and green biomass on a regional scale and integrate the data in geographical information systems (GIS) was of interest to the scientific and wildlife management communities. I used Advanced Very High Resolution Radiometer (AVHRR) to produce daily maps of estimated ground covered by snow and green biomass for the Park.

The advantages of using AVHRR are daily coverage, availability, cost, and historic continuity of the data. The first AVHRR sensor was launched on the TIROS-N (Television Infrared Observation Satellite-National Oceanic and Atmospheric Administration) in 1978. The only significant change in the sensor since 1978 was the addition of a second thermal infrared band in 1981 to improve the correction for water vapor attenuation in the sea surface temperature computations (Hastings and Emery 1992). From 1981 to the retirement of NOAA-10, the satellite making the morning pass had five bands and the satellite making the afternoon pass had four bands. Beginning in 1988, with the launch of NOAA-11, both the morning and afternoon satellites have five bands (Hastings and Emery 1992). Therefore, 10 years of historic data are gained, from 1978 to 1988, if band 4 is used, rather than band 5.

The purpose of the study was to make estimation of snow cover and green biomass automatic and easy to implement for the scientific community and managers interested in regional snow and green biomass cover. Automation was accomplished using an

algorithm, which is a computer procedure with a finite number of discrete steps, to produce an outcome (Berlinski 2000). The algorithm is a folder containing the Navigate program, an Avenue script, and the legend files, which create maps of estimated percent of ground covered by snow and green biomass. Integrating the satellite imagery with GIS allows users to analyze a variety of data types with regional snow or green biomass cover.

The specific objective of this study was to provide the Park with an algorithm that contained two statistically tested models of daily satellite image estimates; one model to estimate percent ground covered by snow (regardless of depth) (% snow cover) and another model to estimate green biomass (kg/ha) in the Park. To achieve this objective, percent snow cover was estimated from photographs taken during two aerial overflights and an index of green biomass was created for 30 sample sites in the Park. Linear regressions between the response variables and pixel values of corresponding satellite images were used to derive the models for the satellite imagery. An algorithm was produced that incorporated the resulting models, image calibration, georeferencing, and a rudimentary method for cloud discrimination.

Several hypotheses, based on previous methods, were tested to find a robust method for estimating snow cover. Fully calibrated and navigated images were expected to estimate ground covered by snow and discern clouds from snow. A combination of bands and topographic characteristics was expected to estimate snow cover and discern clouds from snow. Estimation of green biomass was expected to be determined by models developed by Thoma (1998).

Chapter 1 provides a brief overview of the problem and the hypotheses. Chapter 2 is a literature review concerning remote sensing snow cover and green biomass, along with a description of image processing. Chapter 3 contains a description of the study area and the methods. Chapter 4 summarizes the results of the various methods used to find the optimal methods to estimate snow cover and green biomass. Chapter 5 is primarily a discussion of the results intended to facilitate interpretation of estimated snow cover and green biomass as a result of using the developed algorithm. A brief discussion for future research is included. Chapter 6 is a summary of the study. With the exception of Chapter 6, chapters are divided into sections relevant to snow, green biomass, and image processing.

CHAPTER 2

LITERATURE REVIEW

Snow

Remote sensing studies on various aspects of snow discuss the effects of satellite view angle and solar zenith angle on the data (Dozier and Warren 1982, Hall et al. 1989, Holroyd et al.1989, Carroll 1990, Holroyd and Carroll 1990, Wald 1994, Hall et al. 1995, Lipton and Ward 1997), and some researchers standardize the solar zenith angle to compensate for the variation in response values (Carroll 1990, Lindsay and Rothrock 1993, Jin and Simpson 1999). Increasing elevation can affect the thermal-infrared response due to environmental lapse rate cooling (Barnes and Bowley 1972). The Mie theory and the delta-Eddington approximation were used by Dozier and Warren (1982) to conclude that snow emissivity is similar to a blackbody (emissivity 0.985 – 0.990), and that the infrared emission of snow is not dependent on grain size, density, liquid water content, or the impurity content. The only substantial factor in calculating snow surface temperature from satellite imagery was the viewing geometry. The variations of brightness temperature were attributed to view angle (Dozier and Warren 1982). Subsequent studies measured the directional hemispherical reflectance spectra of snow particles ranging from fine acicular dry snow to coarse granular crust (Salisbury et al. 1994) and compared radiative transfer theories to these results (Wald 1994). Wald (1994) differed in the conclusions put forth by Dozier and Warren (1982). The use of Mie theory

to estimate albedo and asymmetry parameter leads to overestimating the Mie albedo and asymmetry parameter values because in close-packed radiative transfer problems, forward scattered light is indistinguishable from unscattered light. Also, the extinction efficiency of a close-packed particle, where nearest neighbors are closer than the distance of the effective extinction radius, means that the scatter is less than its Mie efficiency. In welded snow, the Mie albedo and asymmetry parameter incorrectly describe snow scattering properties because particles are no longer independent and the number of interfaces between particles is decreased. However, the results upheld previous conclusions that brightness temperature was strongly influenced by the emission angle (Dozier and Warren 1982, Wald 1994). The difference between brightness temperature and kinetic temperature as a function of angle calculated by Dozier and Warren (1982) was similar to models suggested by Wald (1994). Another study found that in mountainous areas when there was a high correlation between satellite view angle and solar zenith angle there was a large positive bias in estimated surface temperature, resulting from direct viewing of the warmest slopes and oblique viewing of the coolest slopes (Lipton and Ward 1997).

Bands 1 (0.58-0.68 μm) and 2 (0.725-1.05 μm) on the AVHRR sensor were designed to discern clouds, land-water boundaries, the extent of snow and ice, and the beginning of snow/ice melt by providing a quasi-linear conversion between the 10-bit digital numbers and albedo. Bands 3 (3.55-3.92 μm), 4 (10.3-11.3 μm), and 5 (11.5-12.5 μm) were designed to measure the temperature of clouds and the sea surface, along with nighttime cloud mapping (Hastings and Emery 1992). The high albedo in the visible spectrum of

snow and the dendritic signatures against the Earth's surface were used to subjectively map the extent of snow by National Oceanic and Atmospheric Administration/National Environmental Satellite, Data, and Information Service (NOAA/NESDIS) (Basist et al. 1996). The Normalized Difference Vegetation Index (NDVI) was of interest because snow has a high albedo in the visible (VIS) range and a lower reflectance in the near-infrared (NIR) range of the spectrum, returning negative numbers for snow covered areas. The difference in the reflection values of snow between the visible and near-infrared bands is used in the equation (NIR – VIS)/(NIR + VIS) to distinguish snow from vegetation and bare ground (Wiscombe and Warren 1980, Dozier 1989, Lillesand and Kiefer 1994). In contrast to snow, green vegetation has relatively low reflectance in the visible band and high reflectance in the near-infrared band, yielding high positive values. Bare ground and rock have similar reflectance in both visible and near-infrared bands, resulting in values near zero, and snow is characterized by low negative numbers (Lillesand and Kiefer 1994).

The Normalized Difference Snow Index (NDSI) is used in the algorithm SNOMAP for the Moderate Resolution Imaging Spectroradiometer (MODIS) data (Hall et al. 1995). The NDSI is based on the difference between snow reflection in the visible and in the mid-infrared part of the spectrum with Landsat Thematic Mapper (TM) bands 2 (0.52-0.60 μm) and 5 (1.55-1.75 μm). Snow reflects strongly in the visible part of the spectrum (TM band 2) and in the region of the spectrum of TM band 5 it reflects less strongly, dropping to near-zero values, while the reflectance of clouds remains high. Therefore, the NDSI distinguishes snow from bright soils and rocks, and functions as a snow/cloud

discriminator (Dozier 1989, Hall et al. 1995). Unfortunately, the AVHRR mid-infrared band 3 (3.55-3.93 μm) is in the part of the mid-infrared that detects contributions from both reflected solar radiation and emitted terrestrial thermal radiation and TM band 5 detects primarily reflected radiation (Holroyd et al. 1989, Holroyd and Carroll 1990). In order to discern clouds from snow, band 4 was subtracted from band 3 (Holroyd et al. 1989, Holroyd and Carroll 1990). This subtraction only roughly represents TM band 5 because the thermal component is not entirely removed from band 3. The reflection from clouds, however, is so much greater than from snow in band 3 that the result was useful for separating snow from clouds (Holroyd et al. 1989, Holroyd and Carroll 1990). To avoid the problem with the thermal component of band 3, Derrien et al. (1993) utilized the differences in reflectance by timing comparisons between bands with the influence of the sun. In an automated algorithm, Derrien et al. (1993) used a series of band combinations and thresholds to detect various cloud types over Europe. The AVHRR images were calibrated to reflectance (1 and 2) and brightness temperature (K) (3, 4, and 5). Band 4 was used to detect medium or high clouds corresponding to low temperature pixels by comparing the cloud pixel brightness temperature to the surface brightness temperature using nighttime images. Cirrus clouds have a greater brightness temperature difference in the subtraction of band 5 from band 4 than cloud-free surfaces. To detect low water clouds in nighttime images, band 3 was subtracted from band 4, the reverse of the equation used by Holroyd et al. (1989). This subtraction was limited to nighttime images because it assumes that at night band 3 is unaffected by solar irradiance. The spectral variation of water cloud emissivity is lower in band 3 than it is in band 4,

resulting in a large brightness temperature difference for small water-particle clouds and a small brightness temperature difference on continental or oceanic surfaces. To detect semi-transparent ice cloud or subpixel cold clouds in nighttime images, band 5 was subtracted from band 3 and a threshold of 3 K was applied. This method was used because the contribution of the relatively warm ground brightness temperature is higher in band 3 than in band 5, due to the lower transmittance of ice clouds and the high non-linearity of the Planck function in band 3 (Derrien et al. 1993). The atmospheric absorption by nitrogen and other gases can be calculated by using differences between the measurements in two spectral regions to account for water vapor absorption and to determine the correct brightness temperature. This is partially due to the atmospheric window where bands 4 and 5 are located (10.5-12.5 μm, band 4 repeated), the principal absorbing agent is water vapor, and in the atmospheric window where band 3 is located (3.5-4.0 μm), water vapor absorption is less than in bands 4 and 5 (Dozier and Warren 1982). In studies of Africa, the brightness temperature threshold was set at 285 K in AVHRR band 5 (10.5-11.5 μm). It was assumed that the surface brightness temperatures in Africa would be above the threshold value and cloud pixel values would be below 285 K. For images with NDVI calculated, the threshold for NDVI pixels was set at zero since cloud pixels usually have brightness temperatures less than the land surface (Holben 1986).

The development of the model for snow cover was based on the argument that linear modeling using multiple non-indexed bands is advantageous in that indices restrain the possibility of individually modeling the singular band responses (Lawrence and Ripple

1998). In a comparison between multiple non-indexed band modeling and several vegetation indices, more variance was explained using stepwise regression and various regression analysis tools on raw band data than using vegetation indices to estimate vegetation cover. Multiple non-indexed band modeling also explained a higher percentage of the variation when shadowing was a factor (Lawrence and Ripple 1998). Elevation, slope, and aspect are relevant in regard to both snow cover and satellite imagery. In the spring at 45°N, snow melts first on the south- and west-facing slopes and later on the north- and east-facing slopes. Snow was found to be bright in sunlit areas, while snow in shadows was as dark as sunlit vegetation and bare ground (Dozier 1989).

Green Biomass

The Normalized Difference Vegetation Index (NDVI) is frequently used in remote sensing vegetation studies (Justice et al. 1985, Lawrence and Ripple 1998). AVHRR band 1 (0.58-0.68 μm), in the visible red, is in a part of the spectrum where chlorophyll absorbs incoming radiation, causing vegetated areas to appear dark with low digital counts. Band 2 (0.725-1.1 μm), in the near-infrared portion of the spectrum, is in the region where spongy mesophyll leaf structure reflects incoming radiation, causing vegetated areas, which have high digital counts, to appear bright (Jensen 1996). The contrast between the two band responses can be represented by a ratio transform. Several ratio transforms are available for studying land surfaces (Justice et al. 1985, Lillesand and Kiefer 1994, Lawrence and Ripple 1998) and the literature is replete with articles on NDVI (Justice et al. 1985, Holben 1986, EROS Data Center 1996, Lawrence and Ripple

1998, Thoma 1998). The NDVI is highly correlated with green leaf biomass and green leaf area, making it a useful tool for vegetation mapping and vegetation discrimination (Holben 1986, Justice and Hiernaux 1986, Box et al. 1989, Kennedy 1989, Lillesand and Kiefer 1994, EROS Data Center 1996, Lawrence and Ripple 1998, Thoma 1998). The equation for AVHRR Normalized Difference Vegetation Index is:

$$NDVI = (b2 - b1)/(b2 + b1)$$

where b1 represents data from the visible band (0.58-0.68 μm) and b2 represents data from the near-infrared band (0.725-1.1 μm) (Justice et al. 1985, Lillesand and Kiefer 1994). A ratio between bands is useful in reducing some variations due to surface topography and in compensating for variations in radiance as a function of sun elevation for different parts of the image (Justice et al. 1985). Atmospheric attenuation was only slightly affected by the ratioing and, therefore, continued to be of concern (Justice et al. 1985, Huete and Tucker 1991). NDVI yields a measure of photosynthetic capacity with the higher value of the ratio indicating more photosynthetically active cover types (Holben 1986). NDVI values theoretically range from 1 to –1, with values of 0.500 representing dense green-leaf vegetation, 0.090 for light green leaf vegetation, 0.025 for bare soil, 0.002 for opaque clouds, – 0.046 for snow and ice, and – 0.257 for water (Holben 1986).

This thesis incorporated the results of a previous study in which estimates of green biomass were derived using EROS bi-weekly composites (Holben 1986, EROS Data Center 1996, Thoma 1998) and ground data from seven grassland study areas in central Montana. Ground data were collected using 0.5 m^2 clip plots clipped at ground level and

sorted into live and dead biomass, dried and weighed. To mitigate the inaccuracy of georeferencing and the large pixel size of AVHRR, 3 km x 3 km ground plots were sampled (Kennedy 1989, Thoma 1998) and pixel values in the 3 km^2 cluster were averaged (Thoma 1998). Models of estimated live green biomass were developed using simple regression between green biomass and NDVI bi-weekly composites. The NDVI bi-weekly composites scale the NDVI to range from 0 to 200 (EROS Data Center 1996). The maximum green biomass for grasslands in Montana was 1800 kg/ha (Thoma 1998), which was similar to the maximum annual green biomass (1806 kg/ha) in the Park (Merrill et al. 1996). Canopy closure occurred in grasslands with green biomass greater than 1800 kg/ha, at which point the signal to background noise ratio limited the ability of NDVI to detect additional green biomass below the closed canopy. This phenomenon is also called a saturation response (Justice and Hiernaux 1986, Thoma 1998). The minimum green biomass detected by NDVI was approximately 250 kg/ha, which is associated with an NDVI of 0.05. Above this lower limit, NDVI is relatively sensitive to changes in green biomass (Justice and Hiernaux 1986, Kennedy 1989, Thoma 1998). Low green biomass levels resulted in low signal to background noise ratios and a breakdown in the ability of NDVI to detect green biomass. Low green biomass thresholds were attributed to minimal coverage of bare ground by plant growth, consequently bare ground dominated the surface (Justice and Hiernaux 1986, Kennedy 1989). The lag time between increasing green biomass and NDVI was found to be less than the lag time between senescing biomass and NDVI (Kennedy 1989). A lag between the onset of green-up and the NDVI response was evident due to the background noise

ratio between bare soil and green vegetation. Early in the green wave, while basal leaves are small, bare ground dominates the response value. As plants mature throughout the growing season, the signature is increasingly dominated by green biomass (Justice and Hiernaux 1986, Huete and Tucker 1991).

Due to the relatively high-quality forage of phenologically young vegetation, ungulates follow the green wave (Frank et al. 1998). This study was concerned with mapping the interface between snowmelt and the onset of phenological development; therefore, the sensitivity of NDVI to increasing green biomass in the spring was critical. Results from studies done on grasslands in Tunisia (Kennedy 1989), Niger (Justice and Hiernaux 1986), Wyoming (Merrill et al. 1993), and Montana (Thoma 1998) report similar correspondence between NDVI values and green biomass. A variety of climates are represented in these studies of semi-arid grasslands, in that precipitation amounts are similar, although the timing of precipitation relative to the growing season varies. The NDVI is similar in Mediterranean dry-summer climates (Christopherson 1997, Kennedy 1989), dry arid and semiarid climates of hot low-latitude steppe in Tunisia (Kennedy 1989) and Niger (Justice and Hiernaux 1986), and in cold mid-latitude steppe (Merrill et al. 1996, Christopherson 1997, Thoma 1998), showing an increase in NDVI with the lag time reflecting the timing of precipitation relative to the growing season (Justice and Hiernaux 1986, Kennedy 1989, Christopherson 1997, Thoma 1998). The congruity between these previous studies on grassland and Thoma's (1998) correlation of NDVI with live biomass, along with the frequent availability of AVHRR, indicate these models potentially fulfill an objective of this study.

The following two equations were evaluated for estimation of green biomass in the Park. Thoma (1998) found that the wet sample site reached a saturation response and eliminated the wet site to improve the coefficient of determination and standard error. The first model (Thoma 1998) includes all seven sample sites:

$$tNDVI7 = 45544 - 728.5ndvi + 2.9ndvi^2$$

where ndvi is the pixel value from the bi-weekly composite, which is NDVI scaled to 0-200 (Adjusted $R^2 = 0.493$, std. error = 875.72, p-value < 0.001, n = 48). For the second model, the wet site was treated as an outlier and eliminated, leaving 6 sample sites:

$$tNDVI6 = -2860.9 + 25.8ndvi$$

(Adjusted $R^2 = 0.640$, std. error = 207.0, p-value < 0.001, n = 36). Note that tNDVI6 is a linear model maintaining the straight line relationship to NDVI, where as tNDVI7 incorporates a quadratic relationship.

Merrill et al. (1996) concluded that although the precision of the model they developed was similar to other models developed for grassland communities, their technique was appropriate for landscape-scale questions, and it was not recommended for more precise estimates. They arrived at this conclusion even though they used imagery of higher spatial resolution (79 m) than AVHRR (1100m). Annual estimates of green biomass for 11 years were derived from Landsat multispectral scanner (MSS) in a northeast area the Park (Merrill et al. 1996). Annual estimations were made from a single MSS overpass each year between 1972 and 1986. A linear regression model based on 25 ground-truth plots sampled in August 1987 was used to determine pixel values for one Landsat MSS overpass during each summer. For a single image the pixel values were averaged across

the study area. A maxima function curve was fit to the annual estimates to account for the average seasonal decline in green biomass from late July to early September. The annual estimation of green biomass ranged from 633 kg/ha on September 2, 1974 to 1806 kg/ha on July 29, 1979. Although senescence was accounted for, the range seems to reflect the senescence of green biomass in late summer. The association of winter precipitation and green biomass was illustrated by a significant quadratic relationship between deviations from the average in annual estimates of green biomass and December-March precipitation. No significant relationship was found between deviations from average green biomass and temperature or total precipitation during the growing season (Merrill et al. 1996), reiterating the need for an algorithm linking snow cover and green biomass.

In Colorado, NDVI was used to investigate the relationship between elevation, slope, aspect, snow deposition, and alpine plant species (Walker et al. 1993). High NDVI values were found on east-facing slopes where moist alpine meadows are typical due to early spring snow melt. Low NDVI values were found on west-facing slopes that are typically wind swept low production sites (Walker et al. 1993). Strong associations were found between snow depth and vegetation communities where fellfield or dry sedge meadow occurred on wind swept west-facing slopes and *Sibbaldia procumbens*, *Trifolium parryi*, and *Carex pyrenaica* occurred on moist east-facing slopes with high snow accumulation (Walker et al. 1993). At a global scale, in regions of complex terrain, such as mountains, NDVI values are suspect due to mixed pixels. Also, relative to global patterns, montane and temperate non-forest sites produce elevated NDVI values (Box et

al. 1989). In mid-latitude regions, above 40° N/S, NDVI is sensitive to a water surface in low-lying areas due to standing water (Box et al. 1989).

Bandwise regression models have been used as an alternative method to vegetation indices (Lawrence and Ripple 1998). Lawrence and Ripple (1998) used linear and log-transformed regressions of separate bands against vegetation cover to ascertain the variable of interest and the bands. A comparison between several vegetation indices and bandwise regression models revealed that regression against raw non-indexed bands explained more variation than the vegetation indices. However, shadow influence was significant for the bandwise regression model and it was not significant for the vegetation indices. Lawrence and Ripple (1998) preferred the use of raw spectral bands as predictor variables and regression analysis to relate spectral responses to the ecological variable, in part because it explained a greater percentage of the variance even when shadowing was a factor.

Image Processing

Image processing was critical to the outcome and interpretation of the study. In this study, the results of a previous study were used in the green biomass estimation and the initial image processing in the two studies was similar, but different. The bi-weekly composites used in Thoma's (1998) thesis are described first, followed by the description of the calibration and georeferencing methods used in this study.

AVHRR data was transmitted from the satellite to the U.S. Geological Survey's EROS Data Center in Sioux Falls, South Dakota, where it was compiled, composited, and

released as Conterminous U.S. AVHRR bi-weekly composites (EROS Data Center 1996). These were composites of presumably cloud-free views over a 14-day period. A maximum-value composite (MVC) procedure using a series of multitemporal georeferenced NDVI satellite images was processed pixel-by-pixel using the highest NDVI value for each pixel location. A final composite image was produced using the highest NDVI value for each pixel from several daily overpasses, which resulted in a nearly cloud free image (Holben 1986). A thermal cloud mask was included by eliminating NDVI data with a value below a designated level. For channels 1 and 2, reflectance channels were converted from raw digital counts to byte data. The reflectance values range from 0 to 254, which represented 0 to 63.5% reflectance. Values greater than 63.5% were grouped into 255. Features with greater than 63.5% reflectance were bright non-vegetated surfaces such as clouds, snow or bare ground (EROS Data Center 1996). The NDVI, ranging from -1.0 to 1.0, was re-scaled to byte data ranging from 0 to 200. Once the NDVI was calculated and re-scaled, the image was georeferenced to the Lambert Azimuthal Equal Area projection. The near-real-time aspect of this study precluded the use of NDVI composites, which introduced the problem of obtaining georeferenced satellite images.

Indirect navigation corrected the image by resampling it to fit the geographic map projection. Georeferencing AVHRR satellite images is referred to as navigation because it both corrects and transforms the image into a known map projection by placing each pixel at the correct geographic location, similar to navigating a vessel (Emery et al. 1989). The georeferenced image can be raw data where the digital number (DN), or raw digital

count, of each band were unaltered, or images can be calibrated, with or without the non-linearity corrections. In the program Navigate, the reflectance bands, visible (1) and near-infrared (2), were calibrated to percent albedo * 10, and the emitted bands, mid-thermal (3) and thermal (4 and 5), were calibrated to brightness temperature (K * 10), using the equations found in Kidwell (1991) and Planet (1988) (Navigate ReadMe undated, Baldwin and Emery 1993). The calibration coefficients were determined by using the pre-launch calibration coefficients contained in the header information of the satellite image; they are unique for each band on individual satellites (Navigate ReadMe undated, Planet 1988, Kidwell 1991). Pre-launch calibration of the reflected bands was performed by integrating the spectral output of a sphere illuminated by 12 quartz-halogen lamps as the maximum illumination and a range of lamps to create a calibration curve of the output ranging from dark to maximum illumination. In-flight, the solar irradiance at the top of the atmosphere was calculated using a similar equation. The percent albedo was calculated as the ratio of the lamp calibration curve and the solar irradiance of the top of the atmosphere. No in-flight calibration was available for the reflected bands (Planet 1988, Kidwell 1991).

For all bands, the calibration coefficients were scaled by dividing the slope values by 2^{30} and dividing the intercept values by 2^{22} (Kidwell 1991). For the reflectance bands, 1 and 2, the input data value was converted to percent albedo by using a linear function of the input data value and the calibration coefficients in the following equation:

$$A_i = S_i C + I_i$$

where A is the percent albedo measured by band i, S_i is the scaled slope of the calibration coefficients, C is the input data value (ranging from 0-1023 counts), and I_i is the intercept value of the calibration coefficient.

For the thermal bands, calibration coefficients were determined from the pre-launch data and in-flight scanning of an internal blackbody (Planet 1988). During the pre-launch calibration, the sensor scanned a warm blackbody representing Earth, a cold target (< 77 K) representing deep space, and the internal blackbody used in the in-flight calibrations. Temperature plateaus were generated from the laboratory blackbody. A quadratic equation was fitted between the scene radiance and AVHRR output count data by least squares regression. In-flight, the radiance of the internal blackbody, which was the baseplate of the sensor equipped with four thermistors or platinum resistance thermometers (PRT) to measure the temperature in counts, was frequently scanned. It was assumed that emissivity had no effect on the radiance or the brightness temperature by setting the emissivity of the laboratory blackbody and the internal blackbody to one.

The process outlined above transferred the calibration of the laboratory blackbody to the internal blackbody through a series of equations. For each thermal band, a linear calibration equation was formulated by regression between the data of the cold target view (radiance assumed to be zero) and the internal target. Radiances were produced using the temperature plateaus of the laboratory blackbody and the application of the linear calibration to the AVHRR output, in counts. The radiances were converted to brightness temperatures using Planck's function over the spectral response function. For the thermal bands, the following equation was applied:

$$E_i = S_i C + I_i$$

where E is the energy value (mW/m^2 sr cm^{-1}). The conversion to brightness temperature used the inverse of Planck's radiation equation:

$$T(E) = C_2 \nu / \ln(1+C_1\nu^3/E)$$

where T is the temperature (K) for the energy value E, ν is the central wave number of the channel filter (cm^{-1}), C_1 is a constant ($1.1910659 * 10^{-5}$ mW/m^2 sr cm^{-4}) and C_2 is a constant (1.4333 cm K) (Kidwell 1991).

In the non-linearity correction step, the difference between the brightness temperatures and the actual temperatures of the laboratory blackbody, determined from the PRT, became the correction terms of each band (Planet 1988). The correction terms were the differences in the subtraction of the brightness temperatures from the actual temperatures of the laboratory blackbody, which were determined from its PRT. The correction term contained both the error term and the emissivity of the blackbodies because the emissivities (ε) of the blackbodies were not measured in the calibration process, therefore, in the following equation:

$$F_r = \varepsilon * \sigma * T_{kin}^4$$

ε is assumed to be one. Emissivity (ε) is the radiant flux from a real material (F_r) divided by the radiant flux of a theoretical blackbody, σ is the *Stefan-Boltzmann* constant ($5.67 * 10^{-12}$ W cm^{-2} K^{-4}), and T_{kin} is the kinetic temperature, which is measured with a thermometer in direct contact with the material (Lillesand and Kiefer 1994, Sabins 1996). The emissivity of a theoretical blackbody is one, however, for all real materials, including the internal and laboratory blackbodies, it is less than one. Emissivity also varies with

wavelength and direction of emission (Lillesand and Kiefer 1994, Sabins 1996). A flag to bypass the non-linearity correction was available in Navigate (Navigate ReadMe undated). Satellite ephemeris data and calibration coefficients were periodically downloaded from a file transfer protocol (ftp) site at the University of Colorado.

The calibrated and raw images were georeferenced using Navigate and Imagine®. Navigate corrected the image and transformed it into a map projection. Several options were available in the Navigate program; however, only the methods relevant to this study were outlined. Ephemeris data in the header of the image was used to indirectly navigate the AVHRR satellite images. In the command line of Navigate, the center point, size as number of pixels, and desired geographic projection for the area of interest was specified. The position and look angle of the satellite were determined from the start time in the satellite image header and a series of iterations further defined the navigation. Georegistration and resampling were combined into one step by mapping the raw digital count or calibrated value of each image pixel to the corresponding measurement in the satellite data using nearest neighbor resampling (Rosborough et al. 1994). In cases where the desired area of the image was off-nadir, Navigate filled in regions stretched by the navigation by repeating pixels and deleted pixels in areas where the pixels were elongated, resulting in pixels that were uniform size throughout the navigated image.

CHAPTER 3

METHODS

Study Area

Yellowstone National Park is located halfway between the equator and the North Pole, bounded by 44.0°N and 45.1°N, and well inland, bounded by 109.7°W and 111.3°W (Despain 1990). It is located primarily in the northwest corner of Wyoming with small areas in Montana and Idaho (Figure 1). The Park is 8,987 km^2, roughly 102 km north to south and 87 km east to west. Eagle Peak, 3462 m, along the eastern boundary, is the highest point; and Reese Creek, 1610 m, near Mammoth Hot Springs on the northern boundary, is the lowest point (Yellowstone National Park 1997). Treeline occurs at approximately 3050 m, and most of the Park is in the subalpine zone between 2125 m and 2750 m (Despain 1990). Average annual precipitation ranges from 26 cm on the northern boundary to 205 cm in the southwest corner. Along the northern boundary, the mean monthly precipitation varies between 1.84 cm in February and 5.67 cm in June, while at the South Entrance the mean monthly precipitation varies between 4.02 cm in August and 11.32 cm in December. From October through May, precipitation is primarily in the form of snow (Skidmore et al. 1994). During 1993, 5 km west of Yellowstone at Hebgen Lake (2013 m), the peak snow accumulation occurred in March and rapid ablation began April 19 (Skidmore et al. 1994). At Old Faithful (64.54 cm) and the South Entrance (82.82 cm), precipitation is slightly greater during the winter in the form of snow than it is

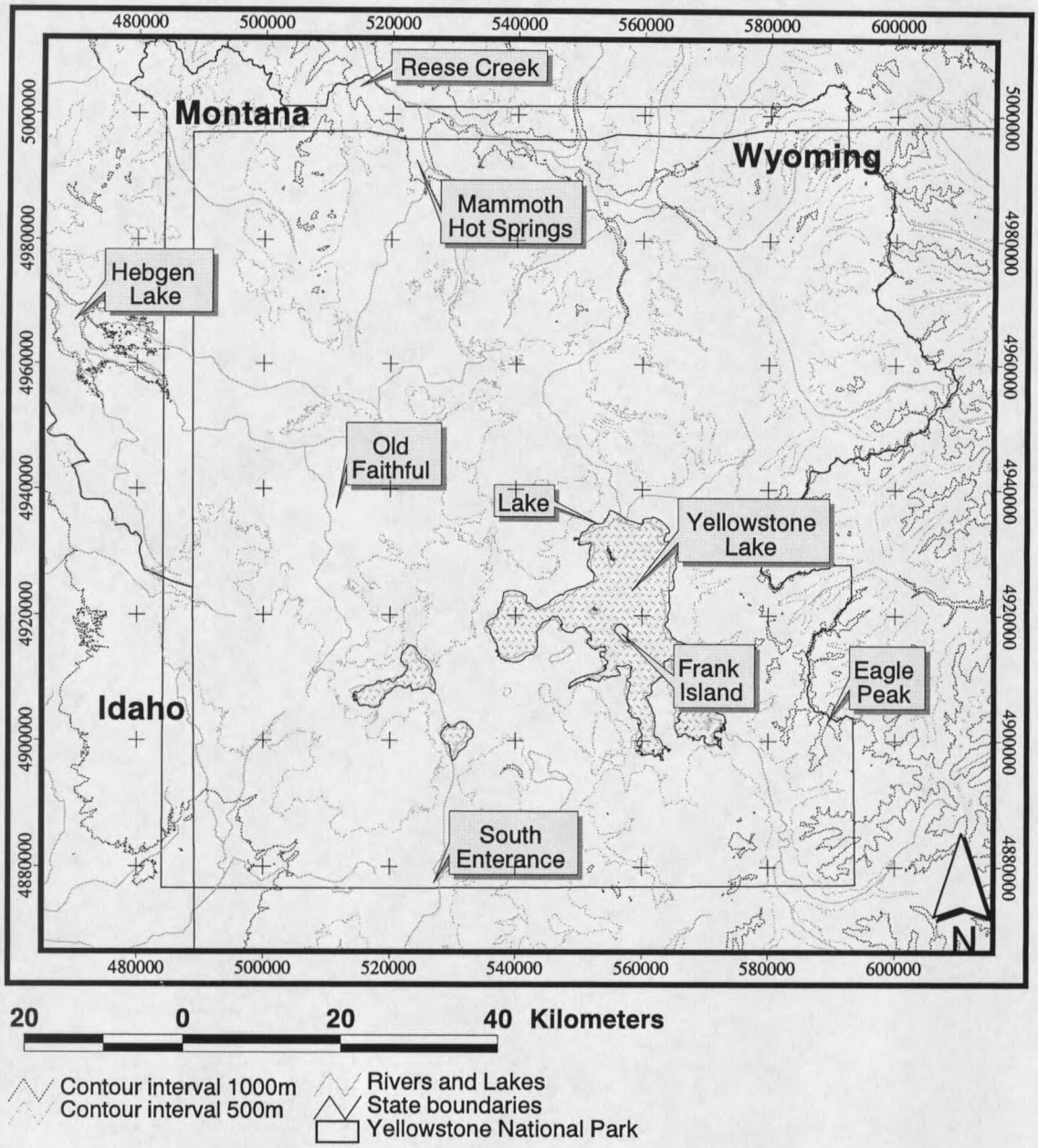

Figure 1. A map of the study area, Yellowstone National Park.

during the summer as rain, and mean annual precipitation is greater than on the northern boundary (39.21 cm). Similarly, the mean monthly temperature on the northern boundary warms above 0°C around April 1, and at Lake it warms above 0°C around May 1 (Western Regional Climate Center, online publication).

Approximately 50 percent of the total annual precipitation falls as snow, which begins melting around April 1. During the next three months, water is released into the soil, and surface waters provide the primary source of moisture to plants during the growing season (Despain 1990). Throughout the summer, thunderstorms produce rain, however, it is not enough to recharge the soil moisture during the growing season. Drought is related to low snow accumulation, rather than lack of rain (Despain 1990). Soil moisture is strongly associated with soil type. Andesitic soils appear to hold moisture throughout the growing season, whereas the high silt rhyolitic soils dry out two weeks to a month before temperatures drop too low for growth. Low silt rhyolitic soils retain only enough soil moisture for a month of the growing season (Despain 1990).

Wildlife in Yellowstone are free ranging and have been subject to a variety of population management regimes since the Park was established in 1872 (Yellowstone National Park 1997). The eight ungulate species in the Park are bison, elk, mule deer, white-tailed deer (*Odocoileus virginianus*), pronghorn, bighorn sheep, moose (*Alces alces*), and mountain goats (*Oreamnos americanus*) (Yellowstone National Park 1990). Other wide-ranging species include grizzly bear (*Ursus arctos*), black bear (*Ursus americanus*), wolf (*Canis lupus*), and mountain lion (*Felis concolor*) (Yellowstone National Park 1990, 1997).

Data Collection

Snow

Calibration data for snow cover was collected using a combination of aerial photography and ground observation. Two flights to collect 35 mm aerial photographs were conducted. The first flight was on April 12, 1999, when 26 observations were collected, and the second flight was on May 6, 1999, when 29 observations were collected, totaling 55 sample sites (Figure 2). Snow cover sample site selection was stratified using a 30 m digital elevation model (DEM) of the Park (Yellowstone National Park online material) and digitized habitat type (Despain 1990) layers in ArcView®. In ArcView®, slope and aspect were derived from the DEM layer. For the pre-flight planning, non-forested habitat types were selected from the habitat type layer to restrict the study to non-forest habitat types. The Universal Transverse Mercator (UTM) coordinates, habitat type, and elevation were recorded and used to assess the flight path. The targeted scale for each slide was 1:46,470 using a 17 mm lens and flying 790 m above the ground. Each slide covered approximately 1626 m x 1069 m, or 1,738,194 m^2 of ground. During the flight, the camera, mounted to a piece of plywood, was pushed out of the airplane through the baggage door. This method was used to avoid photographing the landing gear and wing supports of the airplane for each photograph and control for radial distortion. On April 12, the flight path followed the Yellowstone River drainage to the confluence of the Lamar River and went up the Lamar Valley, turning south toward Pelican Valley (Figure 2, sites 1-26). On May 6, the flight path began in the northwest

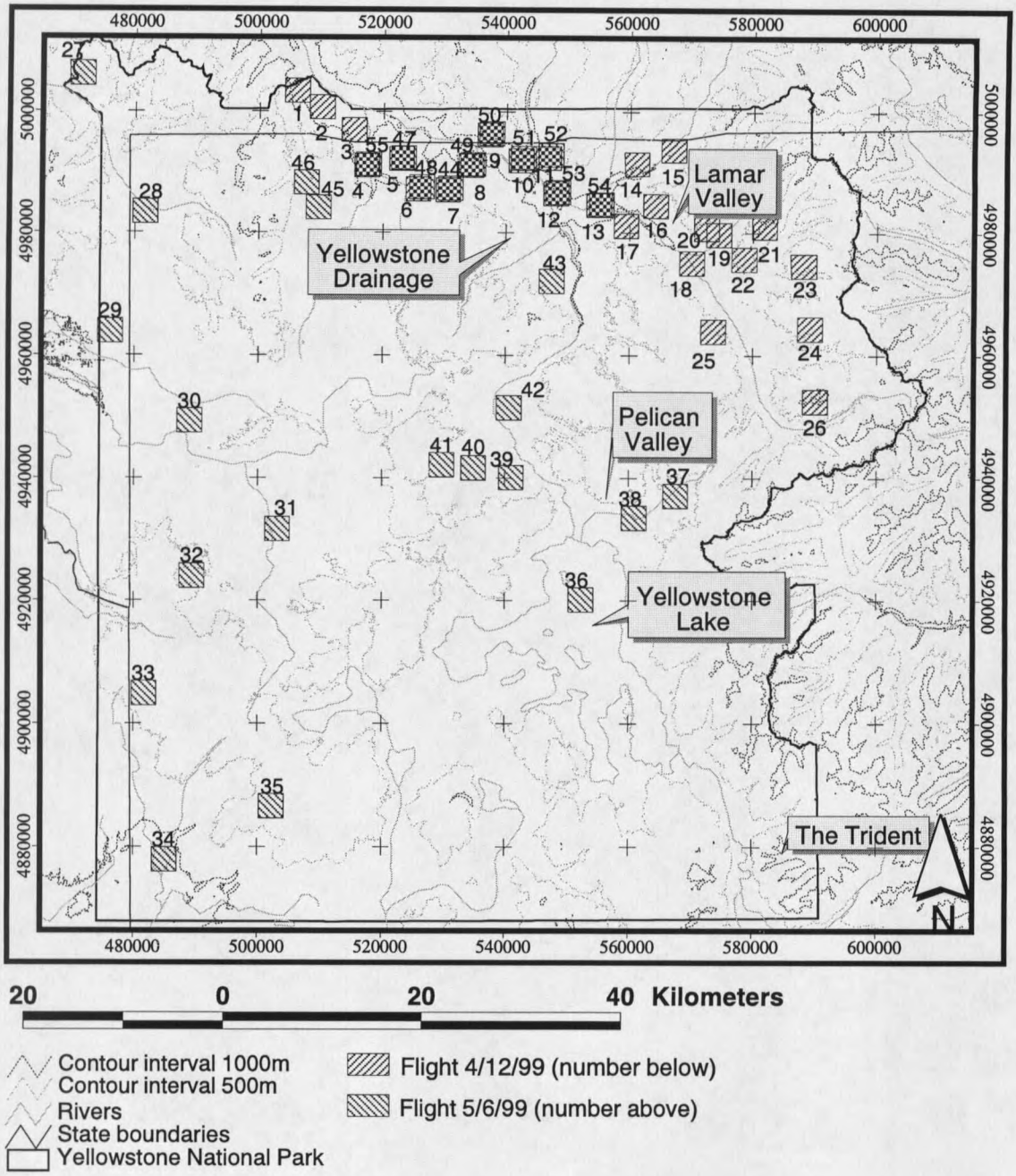

Figure 2. A map of the snow cover sample sites in Yellowstone National Park on April 12 and May 6, 1999.

corner of the Park and went south (Figure 2, sites 27-43). Due to 100 percent snow cover in the southern portion of the Park, particularly The Trident, it was decided to fly back north and look for areas with roughly 50 percent snow cover, which resulted in repeating sample sites in the Yellowstone River drainage (Figure 2, sites 44-55). After each flight, ground based surveys of snow cover were conducted to improve analysis of the photographs.

The slides were analyzed using a point-intercept method and averaging percent snow cover for three or four slides of the sample site. Slides from the flight were analyzed using a Sharper Image Slide Viewer that displayed the slide on a 20 cm x 28 cm daylight screen. A grid of 100 points (1.5 cm squares) was laid over the projected image. The number of points on snow was tallied and the number of points on bare ground was tallied on each slide and recorded separately. The percent of ground covered by snow for each sample site was the average snow covered (ASC) points of the three or four slides corresponding to the sample site. The method was resistant to minor scale variation.

For the final data set, the 30 m DEM of the Park (Yellowstone National Park, online material) was resampled to 1100 m in Arc/INFO GRID® using the nearest neighbor sampling method. Slope and aspect were derived from the resampled DEM using ArcView®. Satellite images corresponding to the date of the overflights were collected and georeferenced. Satellite images were downloaded from the Satellite Active Archive (SAA) website (Satellite Active Archive online material), because the header information was in the format necessary for the Navigate software. Images were used from

NOAA-14, which passed over Yellowstone around 1600 hrs. The satellite was southbound, collecting an image that is oriented with North at the bottom.

Green Biomass

Sample sites were chosen using ArcView® with the Yellowstone DEM (Yellowstone National Park, online material) and the digitized habitat type layer (Yellowstone National Park, online material, Despain 1990). Grassland and shrub habitat types were selected and other habitat types were masked out to eliminate forests from the study. Sites were selected to maximize variation in elevation, slope, aspect, and habitat type, were non-forested and larger than 3 km x 3 km. Much of the commonly identified ungulate habitat, such as in the Lamar Valley, Hayden Valley, and Gibbon Meadows, was between 2001 m and 2500 m in elevation.

The green biomass data were collected in the Park from April through July 1999. Thirty 3 km x 3 km plots were sampled by walking a straight line, with the help of a GPS receiver, between the diagonal corners of each plot (Figure 3). Vegetation cover was estimated for both green herbaceous biomass, including forbs, and shrubs. A modified point-intercept method was used to estimate both components. A "hit" for herbaceous biomass was recorded by estimating ground cover in a 3.75 cm radius circle and the height of the vegetation every 25 paces. At the same point, the shrub component of the estimate was recorded as the ground covered by shrub in a 60 cm radius circle and the height of the tallest shrub within the circle. If there was no vegetation cover within the respective radii, it was recorded as zero, or a "miss." Along each diagonal line, five

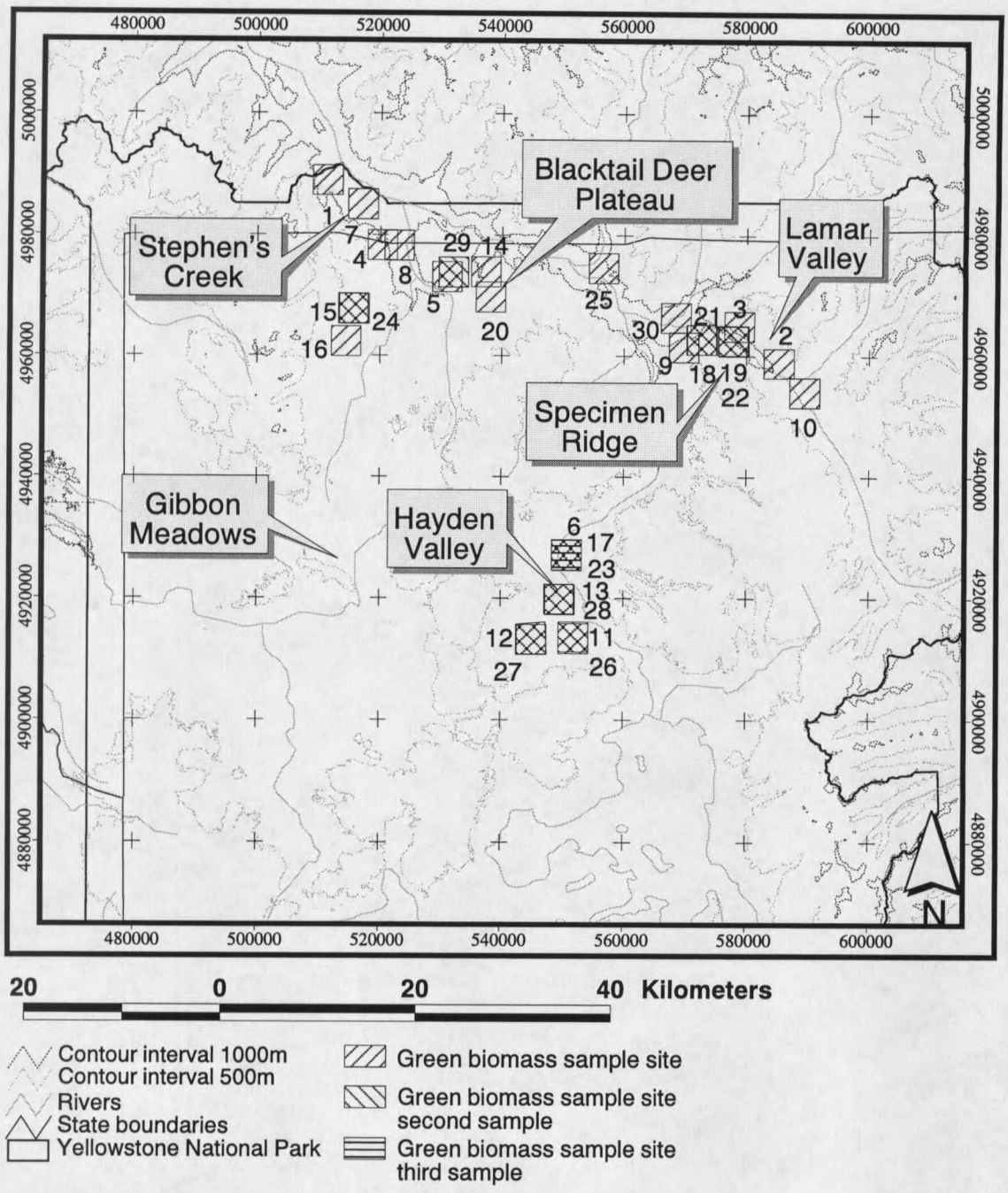

Figure 3. A map of the green biomass sample sites in Yellowstone National Park, April through July 1999.

transects of 500 m each were collected. One diagonal line was sampled by approximately 125 points, which were averaged together. Thirty diagonal lines, 4 km long, were sampled. For each component, the ground cover estimate and the height were multiplied and the products summed for an index number of green biomass, called the green biomass index (GBI). This method combined elements of the line transect and the step-point method. It was chosen as a quick method to estimate green biomass of a large plot by measuring height and percent cover, which has good correlation to standing green biomass (Kűlcher 1967, Kűlcher and Zonneveld 1988). At various points along each diagonal line, UTM coordinates were collected with a GPS receiver. The beginning point and ending point UTM coordinates of the diagonal line were collected for every plot. A center point UTM coordinate was calculated in ArcView® to match the corresponding AVHRR pixel.

Sample sites ranged in elevation from 1591 m to 2426 m and varied in slope and aspect. For example, the Specimen Ridge site had an elevation gain of 440 m and the Hayden Valley sites were relatively flat with the center point UTM coordinate around 2370 m. The lowest sample site was the Stephen's Creek site, which had an elevation gain of 540 m. Sampling was restricted early in the season due to closures for bear, bighorn sheep, and wolf management. Blacktail Deer Plateau was sampled once the area opened on July 1.

Image Processing

Satellite images must be georeferenced to be used as layers in GIS. In a two-part process, on a Sun Solaris Ultra 10 Workstation, a program called Navigate was used to georeference and calibrate the images (Emery et al. 1989, Baldwin and Emery 1993, Rosborough et al. 1994). The second step involved the use of ground control points to project the image in a format that Arc/INFO® and Imagine recognize. The images were corrected to reduce the effects of distortions due to variations in satellite orbit, satellite attitude, earth shape, and earth rotation. Once the images were georeferenced, the pixel to ASCII feature was used to extract the pixel number corresponding to the center UTM coordinate. Depending on the method of image processing, the pixel value was raw digital count (NonNav and NavRaw), calibrated brightness temperature (K * 10) (NavCalFul), or calibrated brightness temperature without the non-linearity corrections (K * 10) (NavCalW/O).

Images were navigated using the command line Navigate described in the literature review. In the command, the options were specified as: Transverse Mercator projection, centered on Frank Island in Yellowstone Lake at 44.28°N and 110.35°W, image size was 512 x 512 pixels with a range of 5°, and the correction for solar zenith. Specification of the image size as 512 x 512 pixels with a range of 5° produced a pixel size approximately 1.1km^2 (Navigate ReadMe undated, Appendix A). In the second part of the georeferencing process, the navigated image was imported into Imagine and georectified using 3-6 ground control points (GCP) with a stream layer developed from the United

States Geological Survey (USGS) digital line graphs (DLG) of streams from Idaho, Montana, and Wyoming (USGS http://www.usgs.gov) in the Universal Transverse Mercator projection, zone 12, and datum NAD83. Most GCP were selected on the edges of the stream layer. The optimal GCP were Boysen and Buffalo Bill Reservoirs and Frank Island in Wyoming, Palisades Reservoir in Idaho, and the confluence of Tom Miner Creek and the Yellowstone River, and Ennis Lake in Montana (Appendix B). The purpose of the georectification in Imagine was to assign a map projection, rather than the rectification of the image because the image was navigated in Navigate.

Snow

To find the optimal algorithm to estimate snow cover, four data sets were created using different image processing methods. The first data set was the raw images georeferenced in Imagine using GCP without Navigate (NonNav). The remaining three data sets used images navigated using options in Navigate and imported into Imagine, layer stacked, and georeferenced with GCP. The second data set used images navigated for georectification and the output was the raw digital count (NavRaw). The third data set used images navigated for location and calibrated with non-linear correction coefficients (NavCalFul), and the fourth data set used images navigated for location and calibrated without non-linear correction coefficients (NavCalW/O) (Navigate ReadMe undated). The percent snow cover, elevation, slope, and aspect were added to the five bands.

Green Biomass

Images were Navigated for location and calibrated with the non-linear corrections because it was critical to emulate the bi-weekly composites used in Thoma's (1998) calculations as much as possible. Three to six GCP were used to georeference the images in Imagine®.

Data Analysis

Snow

For each of the four images, data sets were composed of the percent snow cover estimated from aerial photographs (ASC), the five AVHRR bands, band 3 minus band 4 (sub34), elevation, slope, and aspect. Linear regression was used to test the potential equations and find the optimal band combination to estimate percent snow cover. The results were used to guide further analysis. Stepwise modeling was used to find the regression model with the highest coefficient of determination (R^2) and the fewest predictor variables. Bands 1-5, elevation, slope, and aspect were used in stepwise modeling. Residual plots were used to determine the need for additional regression analysis. Due to the interest in using band 4 in order to utilize images between 1978 and 1988, band 5 was removed from a second stepwise regression.

Based on the literature review, three equations were pieced together in an effort to find a single equation that would estimate snow cover and discern clouds from snow. The NDVI equation (Wiscombe and Warren 1980, Holben 1986, Dozier 1989, Lillesand and Kiefer 1994) was tested using the percent snow cover as the response variable and NDVI

as the predictor variable. The development of SNOWMAP was based on Landsat Thematic Mapper (TM) images (Dozier 1989, Holroyd et al. 1989, Carroll 1990, Holroyd and Carroll 1990, Hall et al. 1995); so available AVHRR bands were substituted into the NDSI equation, resulting in the following equation:

$$\%\ \text{snow cover}_{\text{adaptNDSI}} = [b1-(sub34)]/[b1+(sub34)]$$

where b1 is AVHRR band 1, and sub34 is AVHRR band 3 – band 4. A second equation using sub34 (Holroyd et al. 1989, Carroll 1990, Holroyd and Carroll 1990) was the NDVI multiplied by sub34:

$$\%\ \text{snow cover}_{\text{NDVIsub34}} = [(b2-b1)/(b2+b1)] * sub34$$

where b2 is AVHRR band 2. A stepwise regression with the three equations (NDVI, adaptNDSI and NDVIsub34), sub34, slope, aspect, and elevation as explanatory variables was used to determine the optimal equation.

In addition to selecting a model that is physically relevant, selection of the optimal regression was based on four criteria: a significant overall regression F value and significant slope *t* values ($\alpha = 0.05$), a coefficient of determination greater than 0.50 ($R^2 > 0.50$), and the lowest standard error of the estimate. The desire to use band 4 rather than band 5 so that the algorithm can be used with images between 1978 and 1988 was also a consideration.

Green Biomass

The GBI was added to the five bands in Excel and the NDVI was calculated and rescaled to 0-200, following Thoma (1998), in S-Plus 5.0. To account for the

georectification error and large pixel size, a 3 km^2 plot was sampled, however, unlike Thoma (1998), the pixels were not averaged as 3 km^2 clusters.

Linear regression was used to test the relationship between GBI and the two models reported by Thoma (1998), and GBI and NDVI. The equation tNDVI7 used all seven sample sites, including those with a saturation response and the equation tNDVI6 treated the wet site as an outlier and eliminated it. NDVI was tested primarily as an indicator of the relationship between NDVI and GBI, since tNDVI6 and NDVI are linear.

Algorithm

The algorithm was created once the models were developed and the navigation and calibration method determined. The critical components of the algorithm are the navigation and calibration software and the Avenue script. A ReadMe file, called AlReadMe, containing directions to use the algorithm and information concerning the use and interpretation of the models was also an important component of the algorithm. A copy of the ReadMe and script are provided in Appendix A and C. A directory was created containing the ReadMe (Appendix A), the Navigate program, a figure showing GCP on an image (Appendix B), the script (Appendix C), and the legend files.

Decisions concerning which calibration method to include and the models were made based on the statistical outcome of the regression modeling. Decisions concerning the legend classes and color schemes were based on comparison between images and maps derived using the scripts. The sample site layer provided a reference between navigated

and calibrated images and the maps. Photographs taken during the fieldwork were also a reference source.

The ReadMe was intended to provide the user sufficient information to operate the algorithm and interpret the maps without a copy of this thesis. Relevant sections of the algorithm, results, and discussion are included in the ReadMe, along with detailed directions on the use of Navigate and georeferencing the navigated images.

CHAPTER 4

RESULTS

Snow

The equation that best fit the criteria was:

$$\% \text{ snowcoverb4} = 1261.7543 - 0.4282 * \text{b4}$$

(NavCalFul, Adjusted $R^2 = 0.856$, std. error = 13.60, $\alpha = 0.001$, n = 55) where b4 is AVHRR band 4 using navigated and fully calibrated images (Figure 4, Table 1). Results of stepwise linear regression using the equations derived from the literature were generally less favorable (Adjusted R^2 ranged from 0.729 – 0.824). Using NavRaw digital count images, the equation:

$$\% \text{ snowcover}_{step} =$$

$$-60.8068 - \{1.1941 * [((b2-b1)/(b2+b1)) * (b3-b4)]\} + [0.3851 * (b3-b4)]$$

(NavRaw, Adjusted $R^2 = 0.824$, std. error = 15.2, $\alpha = 0.001$, n = 55), or

(NDVI * sub34) + sub34, was of interest because it was a multiband equation that potentially would discern cloud cover from snow. Stepwise regression with all variables resulted in band 4 using all processing methods except the images calibrated without non-linearity correction (NavCalW/O), which resulted in band 5.

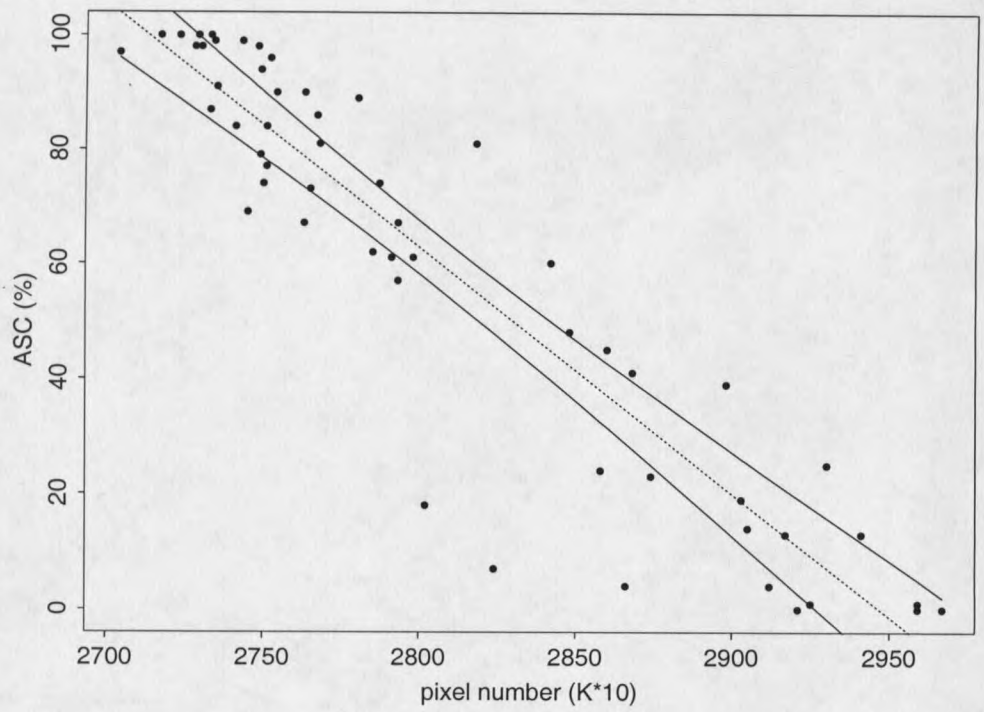

Figure 4. The linear regression model and 95% confidence interval of percent snow cover. The regression model used band 4 with navigated images calibrated with the non-linearity corrections. The linear regression equation is % snowcover_{b4} = 1261.7543 – 0.4282 * b4, where b4 is AVHRR band 4 (Adjusted R^2 = 0.856, std. error = 13.60, α = 0.001, d.f. = 53). The X-axis is the pixel number of navigated and calibrated images and the Y-axis is the average ground covered by snow (ASC).

The images navigated and calibrated with the non-linearity correction (NavCalFul) had the highest coefficient of determination (R^2) and lowest standard error (Table 1). The second highest performing image processing method was navigated raw digital count (NavRaw), followed by raw images (NonNav), and the poorest method was navigated and calibrated without non-linearity corrections (NavCalW/O). All linear regression results were globally significant at the α = 0.05 level and most linear regressions were significant at the α = 0.005 level. Slope and aspect were not significant at the α = 0.05 level.

Table 1. The summary of regression results for estimated snow cover arranged by the four image processing methods considered in Yellowstone National Park, based on flights conducted April 12 and May 6, 1999. Average snow cover (ASC) was the predictor and AVHRR bands and derived equations were the explanatory variables. All reported results were significant for the overall regression and slope coefficient, and the coefficient of determination ($\alpha = 0.05$, $R^2 > 0.500$, $n = 55$).

Explanatory variables	(NonNav) raw image (R^2)	(NavRaw) raw Navigate (R^2)	(NavCalFul) calibrated Navigate with non-linearity (R^2)	(NavCalW/O) calibrated Navigate without non-linearity (R^2)
B1	0.554	0.568	0.651	0.543
B2	0.548	0.574	0.670	0.542
B3	0.717	0.756	0.790	0.678
B4	0.794	0.812	0.856	0.738
B5	0.784	0.808	0.853	0.739
b4 + elevation	0.832	0.839	0.870	–
b5 + elevation	0.830	0.839	0.871	–
NDVI	0.588	0.631	0.699	0.569
adaptNDSI	–	–	0.786	0.635
NDVIsub34	0.589	0.649	–	–

Analysis of the navigated and calibrated singular bands resulted in band 1 with 65% of the variation in the data explained and band 5 with 85% of the variation in the data explained (Table 1). With the exception of NavCalW/O, band 4 had the highest coefficient of determination and lowest standard error of all bands. For the non-calibrated images (NonNav and NavRaw), the slope was positive for all bands, and for the calibrated images (NavCalFul and NavCalW/O), the slope was positive for the reflectance bands and negative for the thermal bands (Figures 5 and 6). The addition of elevation increased the coefficient of determination by 0.01, however, elevation was significant at the $\alpha = 0.005$ level for only the raw images and not for the calibrated images. Analysis of the navigated and calibrated singular bands resulted in band 1 with 65% of the variation in the data explained and band 5 with 85% of the variation in the data explained (Table 1). With the exception of NavCalW/O, band 4 had the highest coefficient of determination and lowest standard error of all bands. For the non-calibrated images (NonNav and NavRaw), the slope was positive for all bands, and for the calibrated images (NavCalFul and NavCalW/O), the slope was positive for the reflectance bands and negative for the thermal bands (Figures 5 and 6). The addition of elevation increased the coefficient of determination by 0.01, however, elevation was significant at the $\alpha = 0.005$ level for only the raw images and not for the calibrated images.

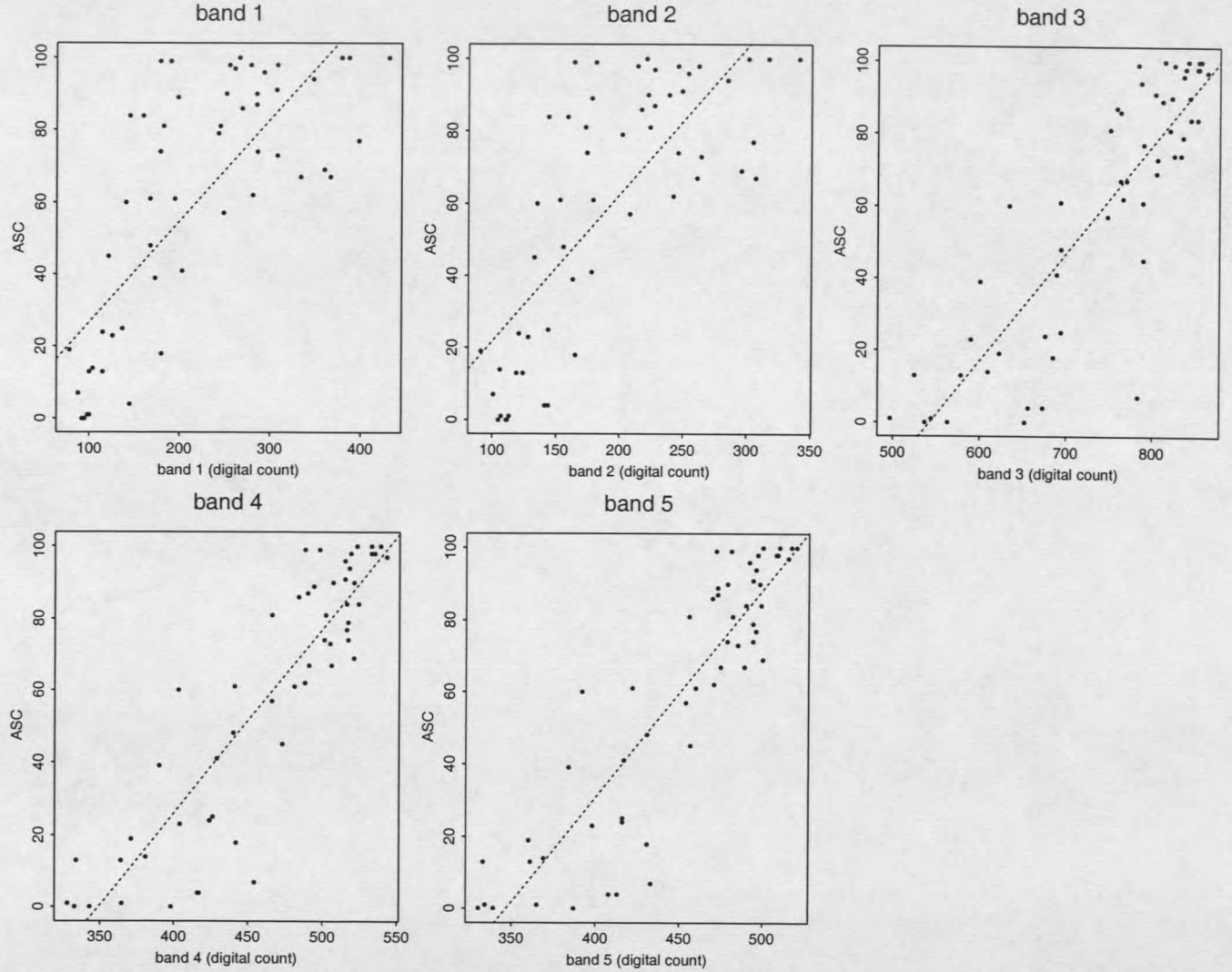

Figure 5. Scatter plots of AVHRR bands 1-5 from navigated raw images for estimated snow cover in Yellowstone National Park, for April 12 and May 6, 1999. ASC is the average ground covered by snow (%) estimated from aerial photographs.

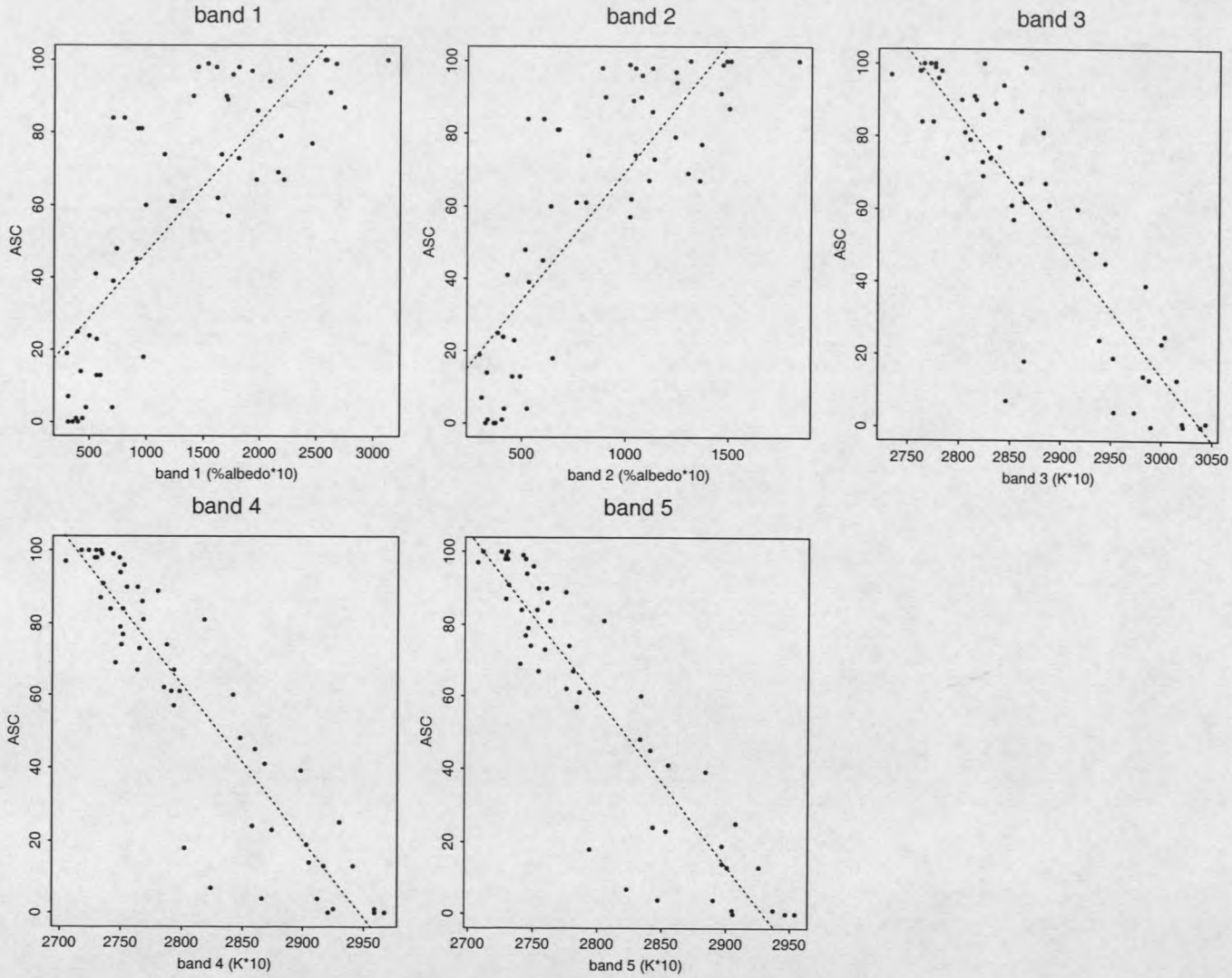

Figure 6. Scatter plots AVHRR bands 1-5 from navigated and calibrated images for estimated snow cover in Yellowstone National Park, for April 12 and May 6, 1999. ASC is the average ground covered by snow (%) estimated from aerial photographs.

Green Biomass

The linear regression of GBI and tNDVI6 (lmtNDVI6) was significant at the $\alpha = 0.005$ level (Adjusted $R^2 = 0.494$, std. error = 27.1, $\alpha = 0.0001$, d.f. = 28, Figure 7). Regression of tNDVI7 on GBI (lmtNDVI7) was also significant at the $\alpha = 0.005$ level (Adjusted $R^2 = 0.349$, std. error = 30.7, $\alpha = 0.001$, d.f. = 28). Due to the linear relationship between NDVI and tNDVI6, regressing NDVI on GBI (lmNDVI) yielded the same results as lmtNDVI6 (Adjusted $R^2 = 0.494$, std. error = 27.1, $\alpha = 0.0001$, d.f. = 28). Dropping one outlier improved the coefficient of determination substantially (lmtNDVI6 and lmNDVI, Adjusted $R^2 = 0.592$, std. error = 24.4, $\alpha = 0.0001$, d.f. = 27, Figure 8; lmtNDVI7, Adjusted $R^2 = 0.403$, std. error = 29.510, $\alpha = 0.001$, d.f. = 27). The outlier dropped was Boiling River (Figure 3, #8), which had a high GBI due to 2 m tall big sagebrush (*Artmesia tridentata*) along the river. Sampling was biased for inflated green biomass because the portion of the diagonal line sampled was in the drainage and the west-facing slope was not sampled due to a bighorn sheep management closure. The equation tNDVI6 best fits the criteria for a correlation between ground data and an estimate of green biomass (Figure 7).

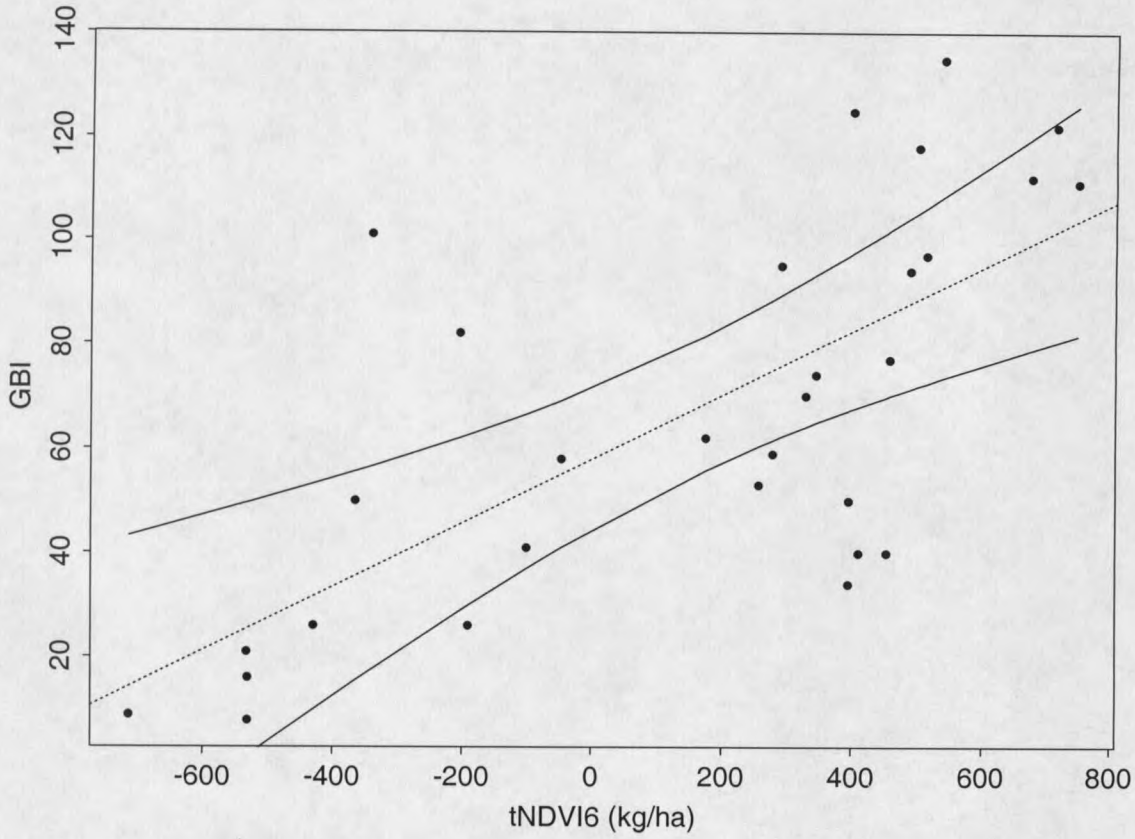

Figure 7. The linear regression model and 95% confidence interval of the estimated green biomass for images of Yellowstone National Park from April 27 to July 25, 1999. The regression model used GBI as the predictor and tNDVI6 as the explanatory variable. The linear regression equation is green $biomass_{tNDVIa6} = 57.9327 + 0.0612 * (tNDVI6)$, where tNDVI6 = -2860.9 + 25.8 * ndvi (the X-axis). The Y-axis is the green biomass index (GBI) (Adjusted $R^2 = 0.494$, std. error = 27.08, $\alpha = 0.0001$, d.f = 28).

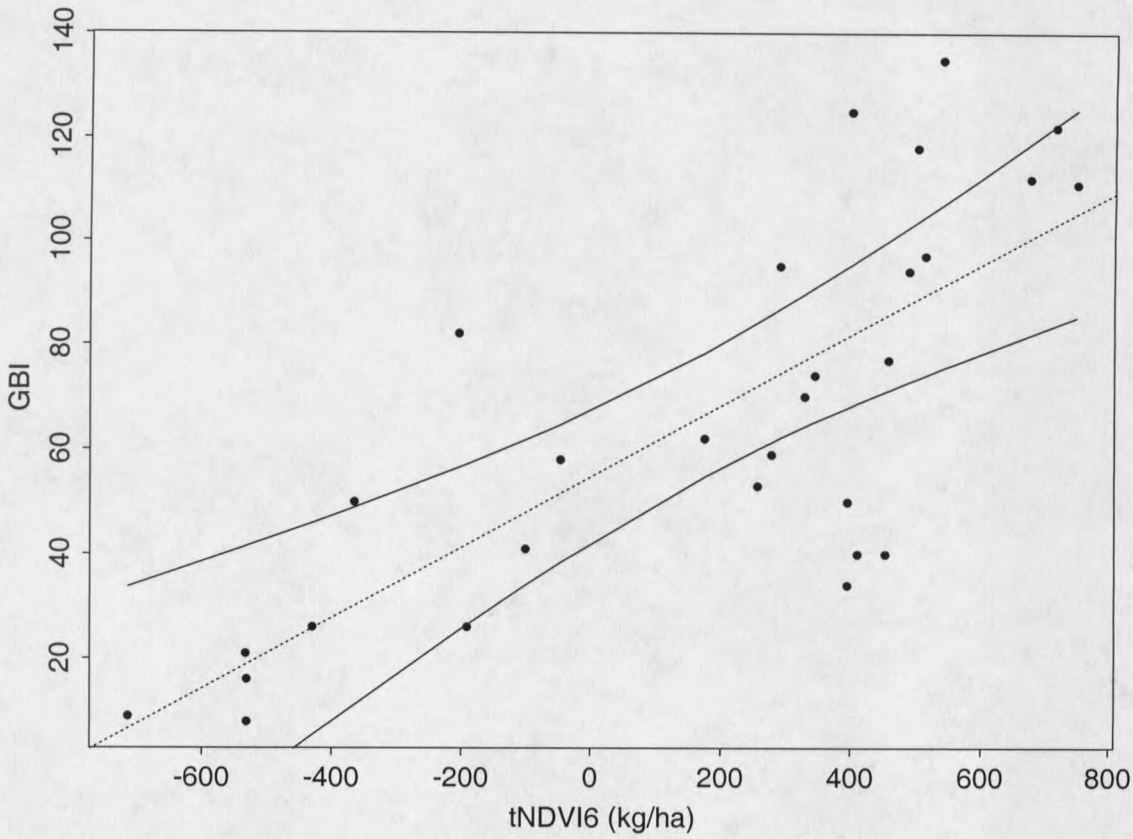

Figure 8. The linear regression model and 95% confidence interval of the estimated green biomass (outlier removed) for images of Yellowstone National Park from April 27 to July 25, 1999. The regression model used GBI as the predictor and tNDVI6 as the explanatory variable. The linear regression equation is green $biomass_{tNDVIc6}$ = 54.7014 + 0.0675 * (tNDVI6), where tNDVI6 = -2860.9 + 25.8 * ndvi (the X-axis). The Y-axis is the green biomass index (GBI) (Adjusted R^2 = 0.592, std. error= 24.4, α =0.0001, d.f. = 27).

CHAPTER 5

DISCUSSION

Snow

Fully calibrated images had the highest coefficient of determination of the image processing methods tested. Images calibrated without the non-linearity corrections (NavCalW/O) consistently had the lowest coefficient of determination (R^2) and images calibrated with the non-linearity corrections (NavCalFul) consistently had the highest R^2. Similarities in performance occurred with calibrated images and raw digital count images, in that elevation was significant at the $\alpha = 0.005$ level for both NonNav and NavRaw, and significant at the $\alpha = 0.05$ level for NavCalFul and NavCalW/O. Although NavCalFul band 4 and elevation had the highest R^2, elevation was not significant at the $\alpha = 0.005$ level.

The inclusion of elevation in the stepwise regression was expected due to environmental lapse rate cooling with increasing elevation (Barnes and Bowley 1972, Lipton and Ward 1997). However, with the calibrated images, elevation improved the coefficient of determination by only 0.01. I parsimoniously chose the simpler model, using only band 4, because there was only a slight increase in the coefficient of determination, and the simpler model was thought to be more robust due to the time dependence of elevation relative to snow cover. An important benefit to using only band 4 was the ability to use the algorithm on AVHRR images from 1978 to present due to the

amount of ungulate location data dating back to the mid-1970s. Additionally, both linear modeling and stepwise linear regression resulted in band 4 as the optimal predictor. Therefore, $snowcover_{b4}$, using fully navigated and calibrated images, was chosen as the best equation for the algorithm (Figure 9).

The use of calibrated images was investigated as a means of broadening the application of the algorithm. It was thought that calibrated images would correct for a portion of the error due to changes in emissivity of snow between early morning when the snow was presumably frozen and late afternoon when it was more likely thawing on the surface. The images that were navigated and calibrated without the non-linearity corrections were included in the study to determine if the non-linearity corrections improved the estimation of snow cover. The calibration method related the digital count from the sensor to the brightness temperature through a process that applied the laboratory blackbody calibration to the in-flight internal blackbody digital count using Planck's function over the spectral response function (Kidwell 1991), which inverted the slope (Figures 5 and 6). Left at this, the calibrated images were possibly more robust for snow cover estimation due to the calibration of the sensors. However, in the non-linearity correction step, the emissivity was considered part of the error term, rather than an explanatory variable. If the emissivity of the laboratory and internal blackbodies had been measured, along with the temperatures, emissivity would have been accounted for in the calibration, rather than subtracted out as part of the error term. The emissivity of any substance is wavelength dependent and varies among bands. Due to the characteristic

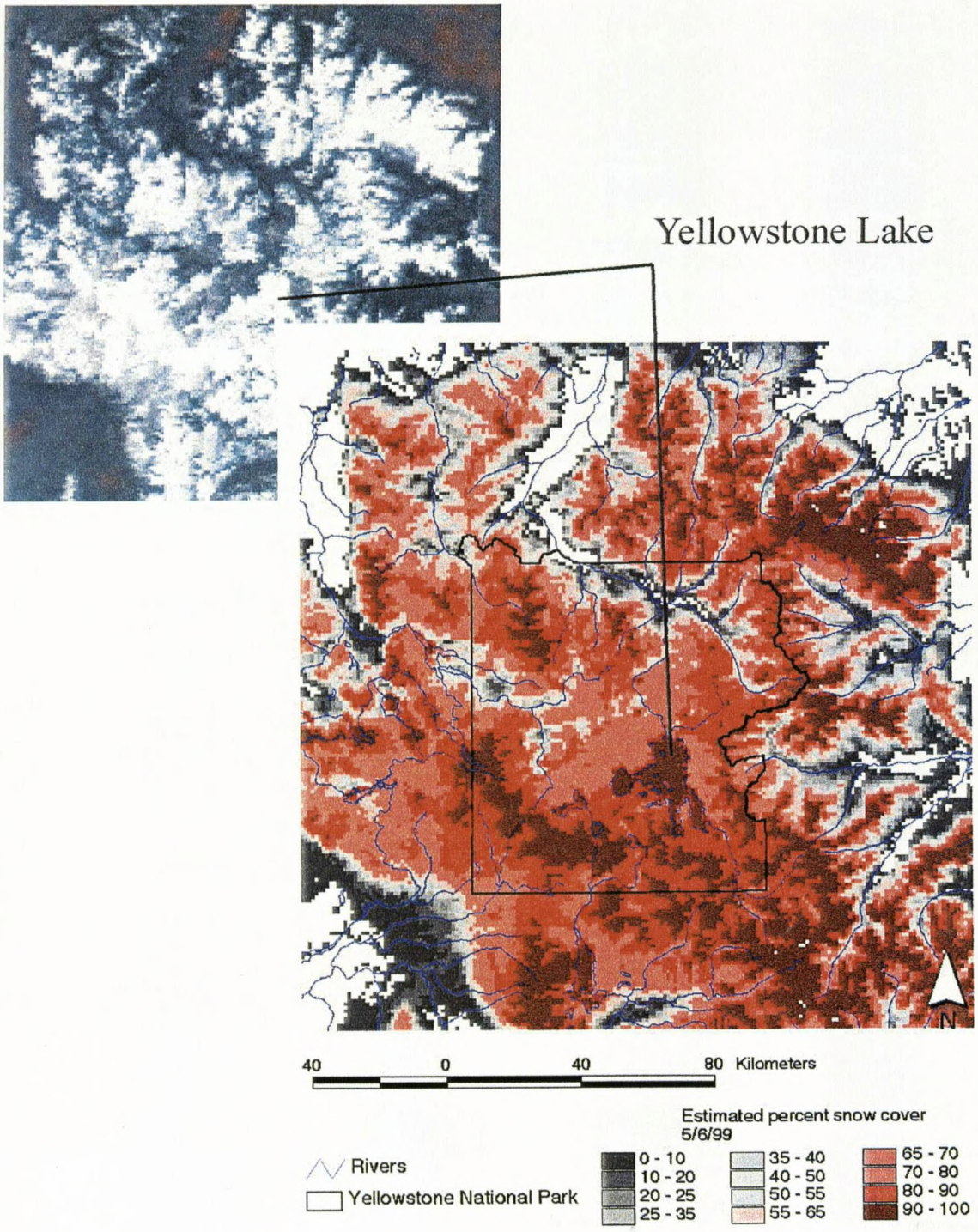

Figure 9. A map of the estimated percent snow cover using the equation $Snowcover_{b4}$ along with the navigated and calibrated image of Yellowstone National Park and surrounding area on May 6, 1999.

emissivity of snow, the retention of emissivity as an explanatory variable could help to distinguish snow from other surfaces (Dozier and Warren 1982, Elachi 1987, Lillesand and Kiefer 1994, Salisbury et al. 1994, Wald 1994). The non-linearity corrections improved the estimation of percent snow cover.

The equations (NDVI, adaptNDSI, NDVIsub34) were tested for two reasons; first, as a comparison with previous work, and second, in an effort to find an equation that would discern clouds from snow. The results of the equations supported the concept that bandwise regression yielded a better model because individual bands were modeled to fit the variable of interest (Lawrence and Ripple 1998). However, the multiband equation, $snowcover_{step}$, using navigated raw digital images (NavRaw), provided a possible avenue to pursue snow cover estimation with cloud discrimination. The equation $snowcover_{step}$ was (NDVI * sub34) + sub34. Based on the literature review, there was some possibility that an equation with several combinations of band subtractions, such as sub34, would both estimate snow cover and discern cloud cover. The difference in percent variation between $snowcover_{step}$ (Adjusted $R^2 = 0.824$) and $snowcover_{b4}$ (Adjusted $R^2 = 0.856$) was only 3%. Data collected for this study were from cloud-free days, which limited evaluation of models for cloud discrimination. Cloud discrimination in the algorithm is discussed in the Algorithm section.

Due to the strong influences of satellite geometry, it was recommended that $Snowcover_{b4}$ be used in conjunction with late afternoon overpasses to be consistent with the conditions it was derived from. The individual band analysis resulted in an increased coefficient of determination as the wavelength increased. For snow in the thermal-

infrared spectral region, most of the spectral radiant emittance occurred between 3 and 70 μm, with the peak at 10.5 μm (Elachi 1987). The Planck blackbody function for characteristic snow surface temperatures peaks between 10 and 11 μm, in band 4 (10.3-11.3 μm) (Dozier and Warren 1982, Hastings and Emery 1992). Wet snow in the spectral range of 8-14 μm had a high absorption, similar to a blackbody and, consequently, it had a high emittance, while dry snow had a lower emittance (Elachi 1987, Lillesand and Kiefer 1994). The measured reflectance of melting snow showed a flattening of the spectrum, with generally increasing emissivity, in the thermal-infrared, and a volume scattering peak in the near-infrared (Salisbury et al. 1994). The variation between snow particle size and packing effects were of secondary importance to the effect of the exitance angle (Dozier and Warren 1982, Wald 1994). The combined effect of satellite viewing angle, solar zenith angle, and terrain, particularly slope and aspect, can result in large differences in surface brightness temperatures (Lipton and Ward 1997). The imagery was from the period of spring snowmelt and was most likely dominated by wet snow because the satellite overpasses were around 1600 hrs on warm spring days. Even so, the satellite geometry dominated the influences on the digital count (Dozier and Warren 1982, Wald 1994). The controlling factor was that the afternoon satellite characteristically passed east of the Park in a descending orbit (North to South) and the sun was in the west, rather than snow condition. Corrections for satellite geometry and solar zenith angle apparently improved percent snow cover estimations (Table 1).

Estimation of percent snow cover is limited to the area of ground covered by snow because the infrared radiation originates within a millimeter of the surface of natural solid

surfaces (Elachi 1987). Therefore, a thin layer of snow might be misinterpreted as a large quantity of snow. It is likely that a thin layer of snow would be estimated as a higher percent snow cover than without the thin snow layer, however, since the pixel size of AVHRR is large and results in mixed pixels, the sensor also detects the bare rock, shrubs, and standing dead vegetation above the snow, which would reduce the percent snow cover estimation.

Green Biomass

Results of the linear regression between GBI and tNDVI6 indicated that the estimated green biomass from tNDVI6 emulate green biomass ground conditions. The equation tNDVI6 explained 64% of the variation in Thoma's (1998) study and 59% of the variation in the Park, which was slightly below the range reported by Lawrence and Ripple (1998).

Green biomass estimates from AVHRR were between 27 kg/ha on May 23 at the Old Gardner Road site (Figure 3, #4) and 907 kg/ha on July 9, 1999 at the Lamar Transect (Figure 3, site #2). The darker red in the July 9 image shows increased vegetation in the upper Lamar Valley, Hayden Valley, and Pelican Valley in the July 9 image (Figure 10). The image on July 9 had the highest average green biomass for the sample period, indicating that the peak green biomass occurred around July 9. However, the July 9 image was brighter than other images, possibly due to atmospheric conditions, creating an interesting effect between increased green biomass and a bright image (Figure 10). Due to the ratioing of NDVI, the effect of the bright image should be lessened by tNDVI6.

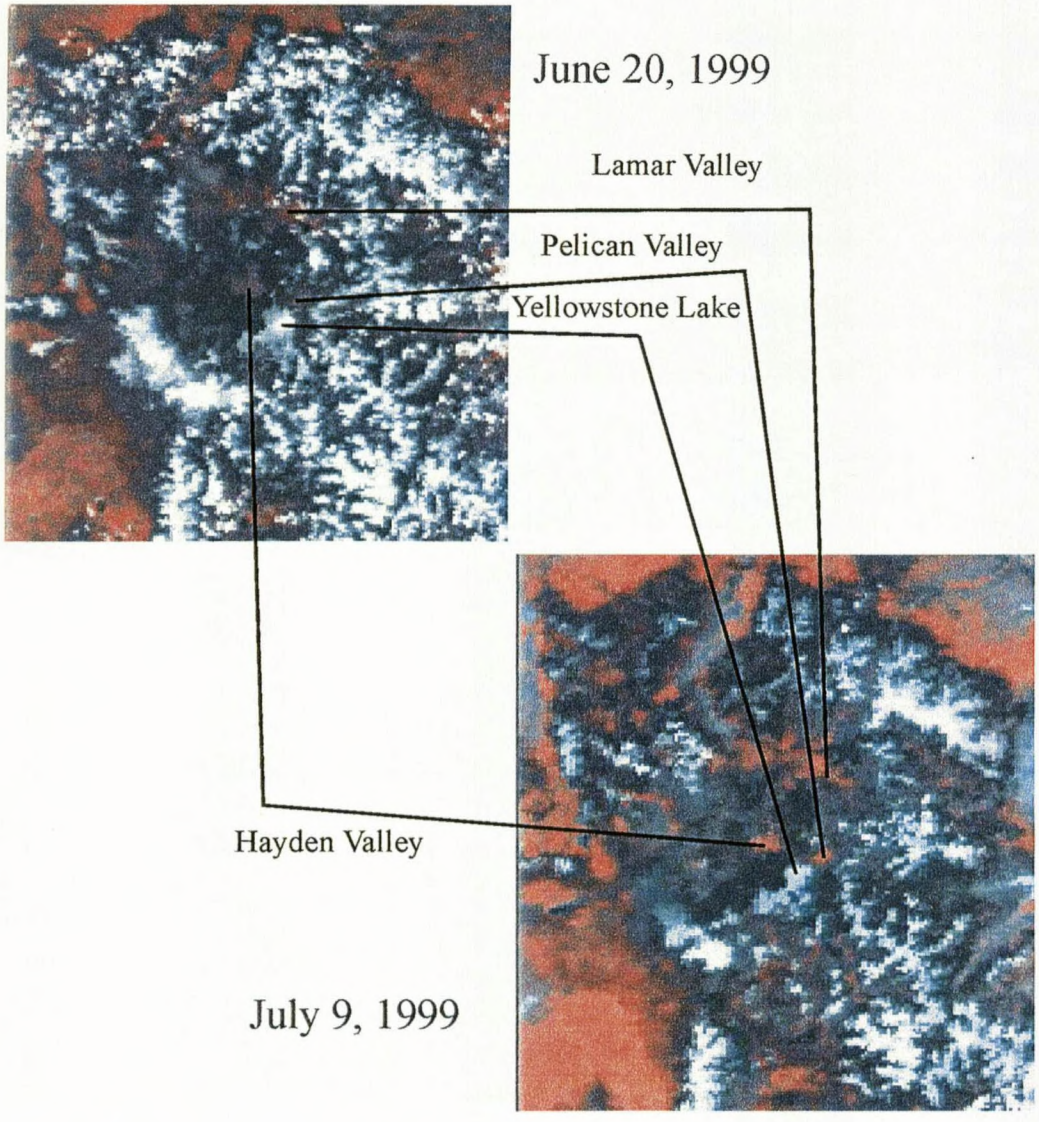

Figure 10. A comparison of the image brightness and green vegetation between images from June 20 and July 9, 1999, of Yellowstone National Park and the surrounding area. Red indicates green vegetation.

Another example of differences in image quality is illustrated in Figure 11, when the June 25 image had cloud cover over a substantial portion of the Park, resulting in lower average daily green biomass estimation.

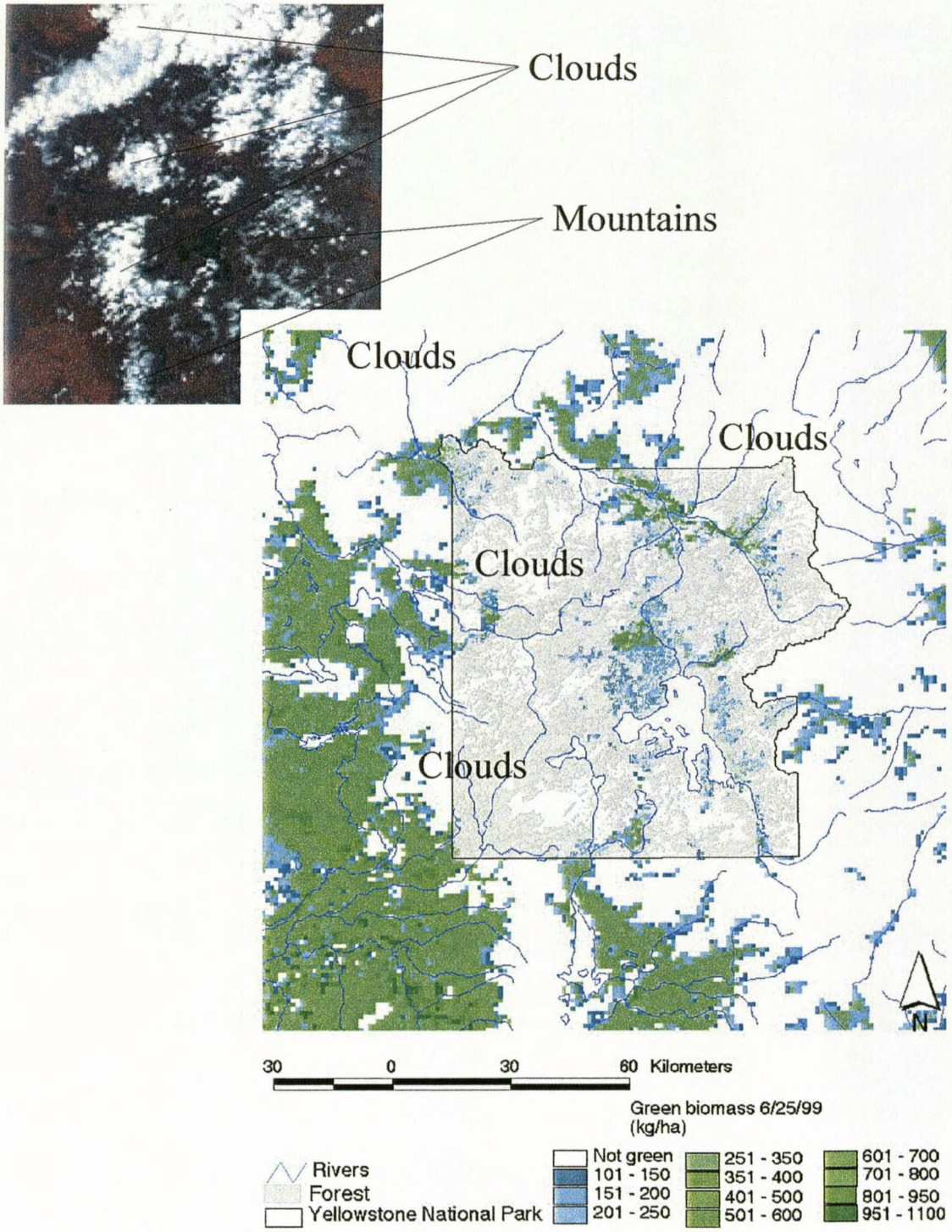

Figure 11. A navigated and calibrated image and the corresponding map of estimated green biomass using tNDVI6 in Yellowstone National Park and surrounding area on June 25, 1999.

The correspondence between field observations and estimates of green biomass was mixed. Comparison between the images and photographs taken during fieldwork indicate a reasonable correspondence between the ground and the images. However, there were some difficulties in assessing the relationship between green up and green biomass estimation from AVHRR images. In early June, it was cloudy and no clear images were available. Therefore, during a critical time for green up, there was a 3-week gap between images for comparison with ground observations. During the return flight on May 6, 1999, Paradise Valley was beginning to green up and the image indicated a few areas were greening (Figure 12). However, pixel values ranging from 101-250 kg/ha are below the lower limit of NDVI (Thoma 1998). There was a discrepancy between values of the lower limit of NDVI. Application of tNDVI6 to the lower limit of NDVI, which was 0.05 (scaledNDVI = 105), yielded a green biomass of 152 kg/ha, and this was well below the observed lower limit of 250kg/ha (Justice and Hiernaux 1986, Kennedy 1989, Thoma 1998). For the most part, the pixels that indicated green up in early May at higher elevations were below the lower limit of 250 kg/ha suggested by previous investigators. This indicated that the NDVI was in a range characteristic of bare ground, clouds, water, and snow (Figure 12) (Justice and Hiernaux 1986, Holben 1986, Kennedy 1989, Thoma 1998). For monitoring early spring green up, the use of the estimated snow cover map as a mask for low estimated green biomass values was recommended.

Varied topography in Yellowstone National Park also accounted for some of the error in estimation of green biomass using AVHRR imagery. The use of NDVI in complex terrain was problematic due to mixed pixels and elevated NDVI values relative to global

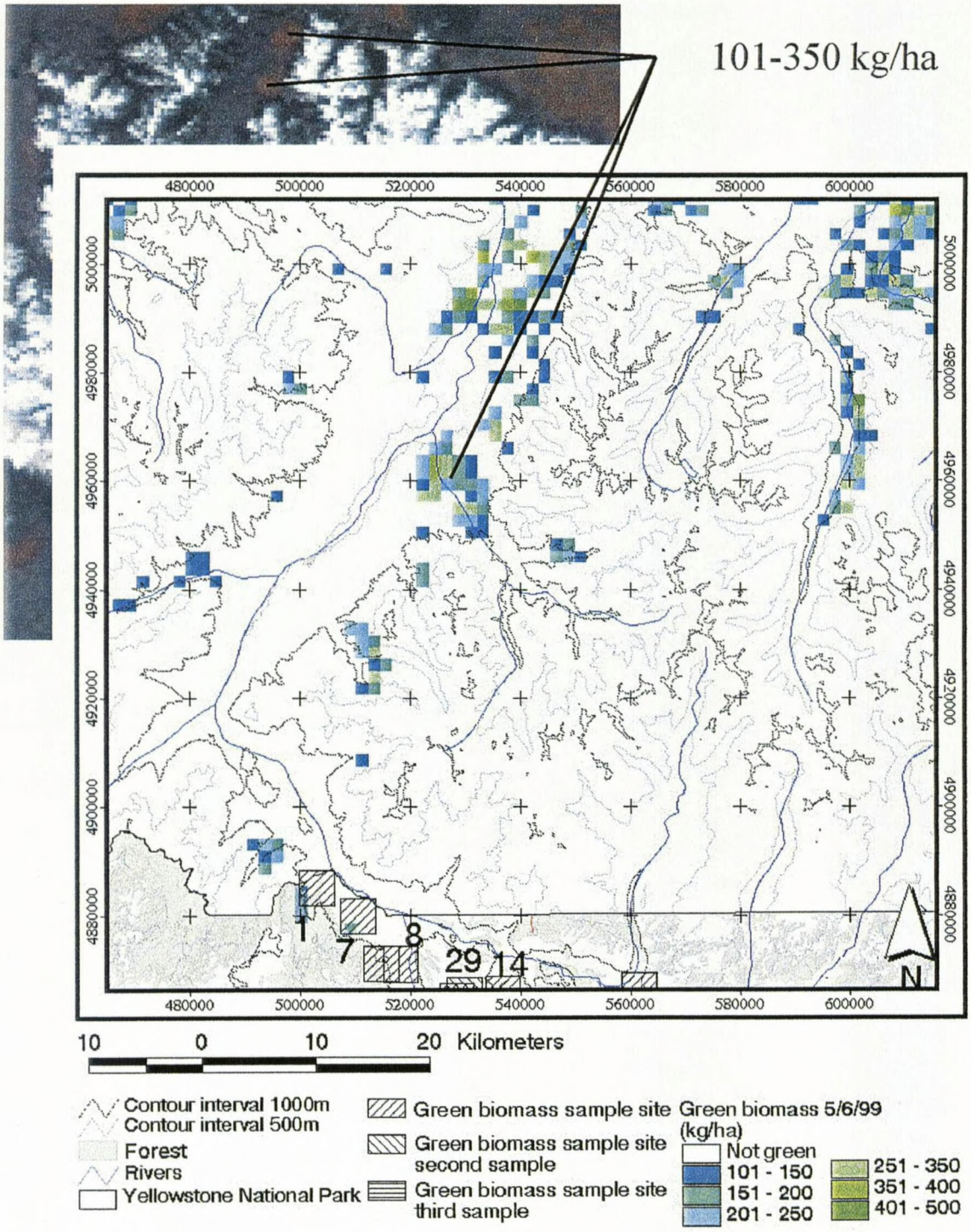

Figure 12. A map of the estimated green biomass in northern Yellowstone National Park and Paradise Valley on May 6, 1999, showing the onset of green up at lower elevations.

NDVI patterns (Box et al. 1989). Although the study by Lipton and Ward (1997) was related to snow cover, the same principle holds, that in mountainous areas there is a high correlation between satellite view angle and solar zenith angle, and the result is a large positive bias in reflectance, due to direct viewing of illuminated slopes and oblique viewing of shadowed slopes (Lipton and Ward 1997). Ratioing indices, such as NDVI account for the correlation between satellite view angle and solar zenith angle by comparing two bands from the same image. Previous studies have found that NDVI mitigates the effect of shadowing (Justice et al. 1995, Lawrence and Ripple 1998), however, NDVI has limitations in regard to satellite view angle, solar zenith angle, topography, and atmospheric condition (Justice and Hiernaux 1986, Huete and Tucker 1991).

Algorithm

The algorithm is contained in a file created to aid in the use of the models for estimation of snow cover and green biomass. The file contains a ReadMe (Appendix A) with directions for using the algorithm and pertinent information concerning its limitations, the Navigate program used to navigate and calibrate images, an image showing the GCP I used to georeference the images (Appendix B), an Avenue script (Appendix C), containing the model for snow cover and green biomass estimation, and the legend files for each grid.

The Avenue script assumes that the grids were raw AVHRR images navigated and fully calibrated using Navigate. Bands 1 and 2 were calibrated to percent albedo * 10,

and bands 3, 4, and 5 were calibrated to K * 10. Images were resampled twice as part of the georeferecing process.

The equations for snow cover and green biomass estimation were put into an Avenue script to be run in ArcView®. The script prompts the user to pick band 1, 2, and 4. Once the bands are picked and $snowcover_{b4}$ runs, the user is prompted to name the estimated snow cover grid. The script runs tNDVI6 and prompts the user to name the estimated green biomass grid. The snow cover equation required band 4 from a navigated and calibrated AVHRR satellite image and it contained the equation $snowcover_{b4}$. A legend file set the $snowcover_{b4}$ values to 20 classes from 0 to 100%, with a gray to red color scale that is consistent for each image. $Snowcover_{b4}$ values above 111 and below - 7 were set as NO DATA and appear the same color as the background (Figure 9). NO DATA might be interpreted as bare ground or cloud cover, depending on the persistence of the NO DATA pattern, since clouds are ephemeral. The 95% confidence interval, ASC, and comparison between images were used to determine these limits.

The green biomass portion of the script involved three steps. The NDVI was calculated and scaled using the equation ((NDVI + 1) / 2) * 200). The green biomass was estimated using tNDVI6. A legend file that converted the tDNVI6 value to a green color scale set the lower limit at 101, with values below 250 kg/ha coded to a blue scale and values above to a green scale. Although the values 101 - 250 kg/ha are questionable, it appeared that setting this range to NO DATA would have missed the onset of green up in Hayden Valley and along the Gardner River. As one might expect, there was overlap between low snow cover and green biomass, when the snow was melting and vegetation

was greening. Rather than set these low ranges to NO DATA, it was left for the user to determine the settings specific to the application. No upper limit was set for the green biomass estimate. It appeared that setting limits for estimated snow cover and green biomass served as a cloud mask (Figure 11). A forest mask was included in the algorithm because the study was conducted in non-forested habitat types. Issues of remotely sensing snow cover in forest were not addressed.

This algorithm was tested with spring snowmelt conditions. Due to the strong influence of satellite geometry and the difference in snow reflectance between morning and late afternoon spring snow, it was recommended that this algorithm be used with AVHRR overpasses of satellites east of the Park in the late afternoon (Wiscombe and Warren 1980, Dozier and Warren 1982, Elachi 1987, Dozier 1989, Lillesand and Kiefer 1994, Lipton and Ward 1997).

Future Research

This study was completed as a precursor to using the archived ungulate data collected in Yellowstone (P. Gogan personal communication) and the archived AVHRR images available from SAA to investigate the correlation between ungulate distribution and snow cover and green biomass. It is recommended that both current and archived data be used to investigate the relationships between ungulate distribution and snow cover and green biomass. Ungulate migration is strongly influenced by snow depth (Sweeney and Sweeney 1984) and this method does not estimate snow depth, only ground covered by snow. Time series analysis, based on the assumption that deeper snow melts later in the

spring than thin snow cover, might be used as a substitute for snow depth. The ability to map snow cover regionally allows a comparison of the availability of bare ground to the distribution of ungulates, as opposed to collecting data on snow cover where ungulates are observed. Likewise, mapping green biomass regionally and comparing the availability of green biomass to ungulate distribution might be informative.

Researchers interested in climate change might use this algorithm in time series analysis to investigate the changes in timing of snowmelt and green up since 1978 in Yellowstone. For instance, based on the hypothesis that green biomass is related to winter snow accumulation, has there been a change in the timing of peak green biomass due to a change in spring snow cover? This algorithm could be used to estimate snow cover for various regional hydrology studies. In conjunction with stream morphology data, the algorithm could be used to investigate physical geographic processes.

Improving the discrimination between snow cover and cloud cover would potentially enhance snow cover estimation. Methods described in Derrien et al. (1993) might be useful in developing a simple and robust method to incorporate into the Avenue script. To improve green biomass estimation, I recommend repeating the same process, but apply Thoma's model to AVHRR bi-weekly composites and regress the results on ground data. This might improve the availability of images during June when green biomass is increasing rapidly and it is cloudy.

CHAPTER 6

CONCLUSION

Band 4 in the equation $Snowcover_{b4}$ worked well to estimate snow cover in Yellowstone National Park. The linear model developed by Thoma (1988) was sufficient to estimate green biomass in the Park. There appears to be some lag time between the on-set of green up and detection by NDVI, which was due to the exposure of bare ground prior to the vegetation covering sufficient ground area to dominate the pixel signal (Justice and Hiernaux 1986, Kennedy 1989, Thoma 1998). To estimate both snow cover and green biomass, it is recommended that the algorithm be used with images from late afternoon overpasses (2100 GMT). With regard to snow, satellite viewing geometry was the most significant source of variation (Wald 1994, Lipton and Ward 1997). Estimation of green biomass using NDVI was also dependent on viewing geometry, however, because NDVI is a ratio of two bands, the affects of surface topography and variations in radiances as a function of Sun elevation are lessened (Justice et al. 1985).

The algorithm requires the software Navigate, software to georeference the images, and ArcView®. An Avenue script containing the equations $snowcover_{b4}$ and tNDVI6 applies the equations to navigated and fully calibrated images in ArcView®. Snow cover and green biomass estimation in the Park is available in a format that can easily be used by wildlife biologists, geographers, and Park managers in further investigations regarding the movements of ungulates.

REFERENCES CITED

Baldwin, D.G., and W.J. Emery. 1993. A systematized approach to AVHRR Image Navigation. *Annals of Glaciology*. 17:414-420.

Barnes, J.C., and C.J. Bowley. 1972. *Snow studies using thermal infrared measurements from Earth satellites*. Department of Commerce National Oceanic and Atmospheric Administration National Environmental Satellite Service. Hammonds Ferry Road, Baltimore, Maryland.

Basist, A., D. Garrett, R. Ferraro, N. Grody, and K. Mitchell. 1996. A comparison between snow cover products derived from visible and microwave satellite observations. *Journal of Applied Meteorology*. pp.163-177.

Berlinski, D. 2000. *The Advent of the Algorithm: the idea that rules the world.* Harcourt, Inc. New York, New York.

Box, E.O., B.N. Holben, and V. Kalb. 1989. Accuracy of the AVHRR vegetation index as a predictor of biomass, primary productivity and net CO_2 flux. *Vegetatio*. 80:71-89.

Carroll, T.R. 1990. Operational airborne and satellite snow cover products of the National Operational Hydrologic Remote Sensing Center. *Proceedings of the Forty-seventh Annual Eastern Snow Conference*. June 7-8, 1990. Bangor, Maine, CRREL Special Report 90-44.

Christopherson, R.W. 1997. *Geosystems: An Introduction to Physical Geography*. Third edition. Prentice Hall, Upper Saddle River, New Jersey.

Despain, D.G. 1990. *Yellowstone Vegetation: Consequences of environment and history in a natural setting*. Roberts Rinehart Publishers. Boulder, Colorado. (http://www.nps.gov/yell/technical/gis/download.htm)

Derrien, M., B. Farki, L. Harang, H. LeGleau, A. Noyalet, D. Pochic, and A. Sairouni. 1993. Automatic cloud detection applied to NOAA-11/AVHRR imagery. *Remote Sensing of Environment*. 46:246-267.

Dozier, J., and S.G. Warren. 1982. Effect of viewing angle on the infrared brightness temperature of snow. *Water Resources Research*. 18:1424-1434.

Dozier, J. 1989. Spectral signature of alpine snow cover from the Landsat Thematic Mapper. *Remote Sensing of Environment*. 28:9-22.

Elachi, C. 1987. *Introduction to the Physics and Techniques of Remote Sensing*. John Wiley & Sons, Inc. USA.

Emery, W.J., J. Brown, and V.P. Novak. 1989. AVHRR image navigation: summary and review. *Photogrammetric Engineering and Remote Sensing*. 8:1175-1183.

EROS Data Center. 1996. Readme.1st, The 1996 Conterminous U.S. AVHRR Biweekly Composites. CD-ROM. National Mapping Division U.S. Geological Survey EROS Data Center. Sioux Falls, South Dakota.

Frank, D.A., and S.J. McNaughton. 1996. The ecology of plants, large mammalian herbivores, and drought in Yellowstone National Park. *Ecology*. 73:2043-2058. Reprinted in: *Effects of Grazing by Wild Ungulates in Yellowstone National Park*. Ed. F.J. Singer. Technical report NPS/NRYELL/NRTR/96-01. U.S. Department of the Interior. National Park Service. Denver, Colorado.

Frank, D.A., S.J. McNaughton, and B.F. Tracy. 1998. The ecology of the Earth's grazing ecosystems: profound functional similarities exist between the Serengeti and Yellowstone. *BioScience*. 48:513-521.

Hall, D.K., A.T.C. Chang, J.L. Foster, C.S. Benson, and W.M. Kovalick. 1989. Comparison of in situ and Landsat derived reflectance of Alaskan glaciers. *Remote Sensing Environment*. 28:23-31.

Hall, D.K., G.A. Riggs, and V.V. Salomonson. 1995. Development of methods for mapping global snow cover using moderate resolution imaging spectroradiometer data. *Remote Sensing of Environment*. 54:127-140.

Hastings, D.A., and W.J. Emery. 1992. The advanced very high resolution radiometer (AVHRR): a brief reference guide. *Photogrammetric Engineering and Remote Sensing*. 58:1183-1188.

Hobbs, N.T., D.L. Baker, J.E. Ellis, and D.M. Swift. 1981. Composition and quality of elk winter diets in Colorado. *Journal of Wildlife Management*. 45:156-171.

Holben, B.N. 1986. Characteristics of maximum-value composite images from temporal AVHRR data. *International Journal of Remote Sensing*. 7:1417-1434.

Holroyd, E.W. III, J.P. Verdin, and T.R. Carroll. 1989. Mapping snow cover with satellite imagery: comparison of results from three sensor systems. *Proceedings of the Fifty-seventh Western Snow Conference*. Fort Collins, Colorado.

Holroyd, E.W. III, and T.R. Carroll. 1990. Further refinements in the remote sensing of snow-covered areas. Presented at the American Society of Photogrammetry and Remote Sensing Annual Meeting. Denver, Colorado. March 1990.

Huete, A.R., and C.J. Tucker. 1991. Investigation of soil influences in AVHRR red and near-infrared vegetation index imagery. *International Journal of Remote Sensing*. 12:1223-1242

Jensen, J.R. 1996. *Introductory Digital Image Processing: A remote sensing perspective.* Second ed. Prentice Hall, Upper Saddle River, New Jersey.

Jin, Z., and J.J. Simpson. 1999. Bidirectional anisotropic reflectance of snow and sea ice in AVHRR channel 1 and 2 spectral regions – Part I: Theoretical analysis. *IEEE Transactions on Geoscience and Remote Sensing.* 37:543-554.

Justice, C.O., and P.H. Hiernaux. 1986. Monitoring the grasslands of the Sahel using NOAA AVHRR data: Niger 1983. *International Journal of Remote Sensing.* 7:1475-1497.

Justice, C.O., J.R. Townshend, B.N. Holben, and C.J. Tucker. 1985. Analysis of the phenology of global vegetation using meteorological satellite data. *International Journal of Remote Sensing.* 6:1271-1318.

Kennedy, P. 1989. Monitoring the vegetation of Tunisian grazing lands using the normalized difference vegetation index. *Ambio.* 18:119-123.

Kidwell, K.B. 1991. *NOAA Polar Orbiter data users guide: TIROS-N, NOAA-6, NOAA-7, NOAA-8, NOAA-9, NOAA-10, NOAA-11, and NOAA-12.* NOAA/NESDIS/NCDC/SDSD. Washington, D.C.

Kűlcher, A.W. 1967. *Vegetation Mapping.* The Ronald Press Company. New York, New York.

Kűlcher, A.W., and I.S. Zonneveld, eds. 1988. *Vegetation Mapping.* Kluwer Academic. Boston, Massachusetts.

Lawrence, R.L., and W.J. Ripple. 1998. Comparisons among vegetation indices and bandwise regression in a highly disturbed, heterogeneous landscape: Mount St. Helens, Washington. *Remote Sensing of Environment.* 64:91-102.

Lillesand, T.M., and R.W. Kiefer. 1994. *Remote Sensing and Image Interpretation.* John Wiley & Sons, Inc. New York, New York.

Lindsay, R., and D. Rothrock. 1993. The calculation of surface temperature and albedo of Arctic sea ice from AVHRR. *Annals of Glaciology.* 17:391-397.

Lipton, A.E., and J.M. Ward. 1997. Satellite-view biases in retrieved surface temperatures in mountain areas. *Remote Sensing of Environment.* 60:92-100.

Merrill, E.H., and M.S. Boyce. 1996. Summer range and elk population dynamics in Yellowstone National Park. Ch 17 in *The Greater Yellowstone Ecosystem: Redefining America's Wilderness Heritage*. Eds. R.D. Kelter and M.S. Boyce. Reprinted in: *Effects of Grazing by Wild Ungulates in Yellowstone National Park*. Ed. F.J. Singer. Technical Report NPS/NRYELL/NRTR/96-01. U.S. Department of the Interior. National Park Service. Denver, Colorado.

Merrill, E.H., M.K. Bramble-Brodahl, R.W. Marrs, and M.S. Boyce. 1996. Estimation of green herbaceous phytomass from Landsat MSS data in Yellowstone National Park. *Journal of Range Management*. 46:151-157. Reprinted in: *Effects of Grazing by Wild Ungulates in Yellowstone National Park*. Ed. F.J. Singer. Technical Report NPS/NRYELL/NRTR/96-01. U.S. Department of the Interior. National Park Service. Denver, Colorado.

National Park Service. 1998. *Draft Environmental Impact Statement for the Interagency Bison Management Plan for the state of Montana and Yellowstone National Park*. Department of the Interior. National Park Service. Denver, Colorado.

Navigate ReadMe. Undated. Navigation software. Nav.doc.ascii. Department of Aerospace Engineering Sciences, University of Colorado. Boulder, Colorado.

Planet, W.G., ed. 1988. *Data extraction and calibration of Tiros-N/NOAA radiometers, NOAA Technical Memorandum NESS 107 - Rev. 1*. U.S. Department of Commerce, NOAA/NESDIS. Washington D.C.

Rosborough, G.W., D.G., Baldwin, and W.J. Emery. 1994. Precise AVHRR image navigation. *IEEE Geoscience and Remote Sensing*. 32:644-657.

Sabins, F.F. 1996. *Remote sensing: Principles and interpretations*. Third edition.W.H. Freeman and Company. New York, New York.

Salisbury, J.W., D.M. D'Aria, and A.E. Wald. 1994. Measurements of thermal infrared spectral reflectance of frost, snow, and ice. *Journal of Geophysical Research*. 99:24235-24240.

Satellite Active Archive. online material. (http://www.saa.noaa.gov)

Singer, F.J. ed. 1996. *Effects of Grazing by Wild Ungulates in Yellowstone National Park*. Technical Report NPS/NRYELL/NRTR/96-01. U.S. Department of the Interior. National Park Service. Denver, Colorado.

Skidmore, P., K. Hansen, and W. Quimby. 1994. Snow accumulation and ablation under fire-altered lodgepole pine forest canopies. Abstracts of the Western Snow Conference. Santa Fe, New Mexico.

Sweeney, J.M., and J.B. Sweeney. 1984. Snow depths influencing winter movements of elk. *Journal of Mammalogy*. 65:524-526.

Thoma, D.P. 1998. *Near real-time satellite and ground based radiometric estimation of vegetation biomass, and nitrogen content in Montana rangelands*. M.S. Thesis. Montana State University-Bozeman. Bozeman, Montana.

Wald, A.E. 1994. Modeling thermal infrared (2-14 μm) reflectance spectra of frost and snow. *Journal of Geophysical Research*. 99:24235-24240.

Walker, D.A., J.A. Halfpenny, M.D. Walker, and C.A. Wessman. 1993. Long-term studies of snow-vegetation interactions: A hierarchic geographic information system helps examine links between species distributions and regional patterns of greenness. *BioScience*. 43:287-301.

Western Regional Climate Center. Online publication. National Weather Service (NOAA). Riverton, Wyoming. http://www.wrcc.dri.edu/cgi-bin/cliF30.pl?wyyell.

Wiscombe, W.J. and S.G. Warren. 1980. A model for the spectral albedo of snow. I: Pure snow. *Journal of the Atmospheric Sciences*. 37:2712-2733.

Yellowstone National Park. Online material. http://www.nps.gov/yell/gis/dem30m.html.

Yellowstone National Park. 1990. *Wolves for Yellowstone?: A report to the United States Congress. Volume II, Research and Analysis*. National Park Service. Mammoth Hot Springs, Wyoming.

Yellowstone National Park. 1997. *Yellowstone's Northern Range: complexity and change in a wildland ecosystem*. National Park Service. Mammoth Hot Springs, Wyoming.

APPENDICES

APPENDIX A

ALREADME

AlReadMe

By Donay Hanson

Table of Contents

A. Introduction

Algorithm

This directory is the result of a M.S. thesis by Donay Hanson in the Remote Sensing Lab and the Department of Earth Sciences at Montana State University-Bozeman. The following ReadMe is a summary of the results and discussion of the thesis, along with directions for operating the algorithm. For greater detail, see Hanson (2000). Two models were created. One model estimates the percent ground covered by snow (regardless of depth)(snow cover) from daily AVHRR satellite images. Another model estimates green biomass using an equation developed by David Thoma at Montana State University in 1998 that estimates green biomass (kg/ha) from daily AVHRR satellite images. The objective of the algorithm is to provide a method that makes the models estimating snow cover and green biomass in Yellowstone National Park available to managers and scientific researchers. The algorithm was created once the two models were developed and the navigation and calibration method was determined. The critical components of the algorithm are the navigation and calibration software and the Avenue script. AlReadMe contains directions to use the algorithm and information concerning the use and interpretation of the models. A folder was created containing AlReadMe, the Navigate program (algorithm/navig), a figure showing ground control points (GCP) on an image (algorithm/gcp.jpg), the script (algorithm/arvcview/sngb.ave), and the legend files (algorithm/arcview/snowcob4.ave and /greenbio.avl).

Decisions concerning which calibration method to include and the models were made based on the statistical outcome of the regression modeling. Decisions concerning the legend classes and color schemes were based on comparison between images and maps derived using the scripts. The sample site layer provided a reference between navigated and calibrated images and the maps. Photographs taken during the fieldwork were also a reference source.

The algorithm runs on a Sun Solaris Ultra 10 Workstation. The code for Navigate might need to be changed slightly to run on other Unix platforms. Navigate is not available for Windows.

Navigate

The program Navigate was developed by oceanic researchers using satellites. They need a method to georeference and calibrate images in areas void of reference points for GCP. The file algorithm/navig/navcommands contains 4 commands specific to this thesis and using the Avenue script to estimate snow cover and green biomass. The complete program for Navigate is in navig. The Navigate ReadMe is navig/nav.doc.ascii. It contains information on the codes for the command lines. The command format to run the program deviated from the commands used in the readme, however, the codes are the same. The first

two commands (beginning with filters/sdsfil and cal_new/calibcomp) ran quickly. The third and fourth commands take a minute or two. If it takes more than 5 minutes to run all 4 commands, then its time to troubleshoot. The first command puts the header into the format for Navigate. The second and third commands calibrate the image and the fourth command navigates the image.

ArcView

The script runs the linear regression models on grids of bands 1, 2, and 4 from the navigated and calibrated images (see sngb.ave). It gives the user an opportunity to name each output grid, and puts the output grid into the viewer with the input grids.

The script contains commands that put the file name of the image used in the script (picked in the dialog box) and the equation for snowcoverb4 and tNDVI6 into the respective comments window in the Theme Properties. Comments from bands 4 and 2 of the image are carried over into the comments for each theme. Band 4 comments go to the snow cover theme and band 2 comments go to the green biomass theme. To access this information, highlight the theme and click on THEME|PROPERTIES. The Comments box is at the bottom of the page. Click in the box and use the arrow keys to view all lines.

B. List of Materials

Sun Solaris Ultra 10 Workstation

Software
- Arc/INFO
- Imagine
- ArcView

C. Directions

1. Get image from Satellite Active Archive (SAA) website (http://www.saa.noaa.gov). Follow the directions on the webpage.
   TIPS:
   -- Avoid NOAA-15 because it is 'dropping bands' and the header is in a format that does not work with Navigate.
   -- Look for satellite overpasses around 2100, which means the satellite went over around 1600 hrs (or 4pm)
   -- Use a large spatial range, for instance 97-111degW and 40-50degN
   -- Use the thumbnail image to verify that both band 2 and band 4 are visible. Get some idea of cloud condition from the thumbnails. Look at the map of the area covered by the image. Does it cover northwest Wyoming?
2. Put the image into the algorithm/navig file
3. Run the 4 commands in algorithm/navig/navcommands file
   TIPS:
   -- COPY the command from the text editor to the command line
   -- Keep a log of the navigation commands as a reference

Import the 5 images into Imagine (maybe Arc/Info) Import images as Generic Binary:

IMPORT
- Type: Generic Binary
- Media: File
- Input File: algorithm/navig

Output File:put band # on the left side of the .img (i.e. band1.img)

IMPORT GENERIC BINARY DATA WINDOW

Change—Data type: to Signed 16 Bit

#Rows: 512

#Cols: 512

Notes: for several images, use the 'Load Options"

If image is banded and unreadable, try using the 'Swap Bytes' button below 'Data Type'

Layer stack imported bands

INTERPRETER|UTILITIES|LAYER STACK

6. Georeference the image layer stack in IMAGINE

Open the algorithm/arcview/strmdlg.shp (change file type at the bottom of the dialog box to Shapefile .shp)

The stream layer strmdlg.shp is projected as UTM, zone 12, NAD83 in Arc/Info

Set background to gray (so that georeferencing icon shows up against background)

Open a second Viewer

FILE|RASTER| add the stacked image to be georeferenced

set band combinations to 2,1,1 (RGB) (or a combination that illustrates features)

RASTER|CONTRAST|HISTOGRAM EQUALIZATION

RASTER|GEOMETRIC CORRECTION

POLYNOMIAL|OK

Leave POLYNOMIAL ORDER set at 1 and close

Leave GCP TOOL REFERNCE SETUP set on 'existing viewer', click OK

Follow directions and click in strmdlg viewer

Projection information of the stream layer comes up. Is this what you want your projection in? click OK

Use about 3 ground control points (GCP) to georeference the image (see gcp.jpg in Imagine or the Image Viewer)

A. Pick GCP on the outer edge of the strmdlg

B. Boysen Reservoir in the lower right corner of the strmdlg is a good start (the reservoir shows up as dark color on image)

C. Frank Island or Buffalo Bill Reservoir are good second points (depends what shows up good on the image)

D. The bend of Yellowstone River, near Tom Miner Creek, is a third point. The river turns around a rock outcrop that shows up on the inside of the bend.

E. Pick a fourth point that you are fairly confident you know where the point should be and check the location when it appears on the stream layer. This is an indication of the quality of the georeferencing thus far. Frank Island or the shore of Yellowstone Lake work well.

F. If you are relatively satisfied with the result, save the georeferenced image, but do not close the georeferencing session.

G. Open a third viewer and check the new image with the strmdlg layer. The image is well georeferenced if the rivers follow the drainages. Check the lakeshores and islands in Yellowstone Lake and Jackson Lake.

H. Use the georeferenced image to help pick out other reservoirs, such as Ennis Lake, a smaller lake in the upper left corner of the strmdlg, and refine the placement of the first 3-4 points. Notice the placement of the new GCP. Move south and put a GCP on the Snake River where it enters Palisades Reservoir (this is about 6-7 GCP)

I. Repeat step F and save your georeferenced image to

the same file as F (you can leave the third viewer open and compare the second attempt to the first attempt, by opening a fourth viewer. Caution: make sure you are putting the second georeferenced image into the same file, not the layer stacked image you are georefencing)

J. If it looks good, then stop and EXIT the geometric correciton tool. Not satisfied, repeat the last few steps, add another GCP or two.

NOTE: Georeferencing requires practice. The georeferncing is a significant source of error in the estimation of snow cover or green biomass.

5. Import the georefernced layer stack into Arc/Info:
   imagegrid <file name.img> arcview/file name
 in ArcView
7. Open layers 1,2, and 4
8. Open a Script box and 'Load Text File' algorithm/arcview/sngb.ave
9. Click on the view with the image layers in it
10. Click on the script box and 'run'
11. Follow the directions in the dialog box and pick band 1 (usually ends with c1), pick band 2 (ending c2), pick band 4 (ending c4). The script runs and shows a dialog box asking you for a file name for the grid. If you want to save the grid, type in the name of the file. I use the image date and sn for snow or gb for green biomass so that I can tell by the file name what the image is and some idea of its origin.
12. Double click on the snow cover theme to get the legend dialog box. Load the snowcovb4.avl file and click APPLY
13. Double click on the green biomass theme to get the legend dialog box. Load the arcview/greenbio.avl file and click APPLY
14. Add forestm.shp to view
15. Develop maps in ArcView

Or use Imagine or Arc/Info to pick pixel values of either snow cover or green biomass using UTM coordinates to use in linear regression.

D. METHODS

Snow

Ground data were collected by flying over Yellowstone National Park and taking slides on April 12 and May 6, 1999. Each sample site covered an area approximately 3km x 3km. The point-intercept method was used to determine the average area of ground covered by snow (ASC) by counting the points on a 100-point grid that were on snow and averaging slides (3-4 slides/sample site). Several images processing methods were tested and the one that provided the best results is used in the algorithm. Linear regression was used to determine which combination of pre-processing method, bands, and topographic characteristics produced the model with that with a p-value < 0.05, a high R^2, and a low standard error.

Green Biomass

Ground data for green biomass (GBI) were collected between April 25 and July 25, 1999. Sample sites were 3km x 3km to mitigate the affects of large pixel size and inaccurate georeferencing inherent in AVHRR imagery. A diagonal line, from opposite corners of the 3km x 3km square was walked and height and cover were estimated for shrubs and herbaceous biomass, including grass and forbs. The sample method was a combination of the line transect and the step-point method, measuring height and percent cover, which has good correlation to standing green biomass. Each sample site included approximately 135 points.

Linear regression was used to test the correlation between the GBI and green biomass estimated by David Thoma's (1998) equation. tNDVI6 = -2860.9 + 25.8 * ndvi, where is the ndvi is the NDVI scaled to

0-200 (Adjusted R^2 = 0.640, std. Error = 207.0, p-value < 0.001, n = 36).

E. RESULTS

Snow

The equation that best fit the criteria was:

% snowcoverb4 = 1261.7543 - 0.4282 * b4

(NavCalFul, Adjusted R^2 = 0.856, std. error = 13.60, alpha = 0.001, n = 55) where b4 was AVHRR band 4 using navigated and fully calibrated images. Results of stepwise linear regression using the equations derived from the literature were generally less favorable (Adjusted R^2 ranged from 0.729 - 0.824).

Green Biomass

The linear regression of GBI and tNDVI6 (lmtNDVI6) was significant at the alpha = 0.005 level (Adjusted R^2 = 0.494, std. error = 27.1, alpha = 0.0001, d.f. = 28). Due to the linear relationship between NDVI and tNDVI6, regressing NDVI on GBI (lmNDVI) yielded the same results as lmtNDVI6 (Adjusted R^2 = 0.494, std. error = 27.1, alpha = 0.0001, d.f. = 28). Dropping one outlier improved the coefficient of determination substantially (lmtNDVI6 and lmNDVI, Adjusted R^2 = 0.592, std. error = 24.4, alpha = 0.0001, d.f. = 27). The outlier dropped was Boiling River, which had a high GBI due to 2 m tall big sagebrush (Artmesia tridentata) along the river. Sampling was biased for inflated green biomass because the portion of the diagonal line sampled was in the drainage and the west-facing slope was not sampled due to a bighorn sheep management closure. The equation tNDVI6 best fits the criteria for a correlation between ground data and an estimate of green biomass.

F. DISCUSSION

Snow

The use of calibrated images was investigated as a means of broadening the application of the algorithm. It was thought that calibrated images would correct for a portion of the error due to changes in emissivity of snow between early morning when the snow was presumably frozen and late afternoon when it was more likely thawing on the surface. The images that were navigated and calibrated without the non-linearity corrections were included in the study to determine if the non-linearity corrections improved the estimation of snow cover. The calibration method related the digital count from the sensor to the brightness temperature through a process that applied the laboratory blackbody calibration to the in-flight internal blackbody digital count using Planck's function over the spectral response function (Kidwell 1991), which inverted the slope. The non-linearity corrections improved the estimation of percent snow cover.

The inclusion of elevation in the stepwise regression was expected due to environmental lapse rate cooling with increasing elevation (Barnes and Bowley 1972, Lipton and Ward 1997). However, with the calibrated images, elevation improved the coefficient of determination (R^2) by only 0.01. I parsimoniously chose the simpler model, using only band 4, because there was only a slight increase in the coefficient of determination, and the simpler model was thought to be more robust due to the time dependence of elevation relative to snow cover. An important benefit to using only band 4 was the ability to use the algorithm on AVHRR images from 1978 to present due to the amount of

ungulate location data dating back to the mid-1970s. Additionally, both linear modeling and stepwise linear regression resulted in band 4 as the optimal predictor. Therefore, $snowcover_{b4}$, using fully navigated and calibrated images, was chosen as the best equation for the algorithm.

Due to the strong influences of satellite geometry, it was recommended that $Snowcover_{b4}$ be used in conjunction with late afternoon overpasses to be consistent with the conditions it was derived from. The combined effect of satellite viewing angle, solar zenith angle, and terrain, particularly slope and aspect, can result in large differences in surface brightness temperatures (Lipton and Ward 1997). The imagery was from the period of spring snowmelt and was most likely dominated by wet snow because the satellite overpasses were around 1600 hrs on warm spring days. Even so, the satellite geometry dominated the influences on the digital count (Dozier and Warren 1982, Wald 1994). The controlling factor was that the afternoon satellite characteristically passed east of the Park in a descending orbit (North to South) and the sun was in the west, rather than snow condition. Corrections for satellite geometry and solar zenith angle apparently improved percent snow cover estimations.

Green Biomass

Results of the linear regression between green biomass index (GBI) and tNDVI6 indicated that the estimated green biomass from tNDVI6 reflected green biomass ground conditions. The equation tNDVI6 explained 64% of the variation in Thoma's (1998) study and 59% of the variation in the Park, which was slightly below the range reported by Lawrence and Ripple (1998).

Green biomass estimates from AVHRR were between 27 kg/ha on May 23 at the Old Gardner Road site and 907 kg/ha on July 9, 1999 at the Lamar Transect. In false color composite images (2,1,1), the darker red in the July 9 image shows increased vegetation in the upper Lamar Valley, Hayden Valley, and Pelican Valley in the July 9 image. The image on July 9 had the highest average green biomass for the sample period, indicating that the peak green biomass occurred around July 9. However, the July 9 image was brighter than other images, possibly due to atmospheric conditions, creating an interesting effect between increased green biomass and a bright image. Due to the ratioing of NDVI, the effect of the bright image should be lessened by tNDVI6. Another example of differences in image quality occurred when the June 25 image had cloud cover over a substantial portion of Yellowstone, resulting in lower average daily green biomass estimation.

The correspondence between field observations and estimates of green biomass was mixed. Comparison between the images and photographs taken during fieldwork indicate a reasonable correlation between the ground and the images. However, there were some difficulties in assessing the relationship between green up and green biomass estimation from AVHRR images. In early June, it was cloudy and no clear images were available. Therefore, during a critical time for green up, there was a 3-week gap between images for comparison with ground observations. During the return flight on May 6, 1999, Paradise Valley was beginning to green and the image indicated a few areas were greening. However, pixel values ranging from 101-250 kg/ha are below the lower limit of NDVI (Thoma 1998). There was a discrepancy between values of the lower limit of NDVI. Application of tNDVI6 to the lower limit of NDVI, which was 0.05 (scaledNDVI = 105), yielded a green biomass of 152 kg/ha, and this was well below the observed lower limit of 250kg/ha (Justice and Hiernaux 1986, Kennedy 1989, Thoma 1998). For the most part, the pixels that indicated green up in early May at higher elevations were below the lower limit of 250 kg/ha suggested by previous investigators. This

indicated that the NDVI was in a range characteristic of bare ground, clouds, water, and snow (Figure 12) (Justice and Hiernaux 1986, Holben 1986, Kennedy 1989, Thoma 1998). For monitoring early spring green up, the use of the estimated snow cover map as a mask for low estimated green biomass values was recommended.

Varied topography in Yellowstone National Park also accounted for some of the error in estimation of green biomass using AVHRR imagery. The use of NDVI in complex terrain was problematic due to mixed pixels and elevated NDVI values relative to global NDVI patterns (Box et al. 1989). Although the study by Lipton and Ward (1997) was related to snow cover, the same principle holds, that in mountainous areas there is a high correlation between satellite view angle and solar zenith angle, and the result is a large positive bias in reflectance, due to direct viewing of illuminated slopes and oblique viewing of shadowed slopes (Lipton and Ward 1997). Ratioing indices, such as NDVI account for the correlation between satellite view angle and solar zenith angle by comparing two bands from the same image. Previous studies have found that NDVI mitigates the effect of shadowing (Justice et al. 1995, Lawrence and Ripple 1998), however, NDVI has limitations in regard to satellite view angle, solar zenith angle, topography, and atmospheric condition (Justice and Hiernaux 1986, Huete and Tucker 1991).

Algorithm

The Avenue script assumes that the grids were raw AVHRR images navigated and fully calibrated using Navigate. Bands 1 and 2 were calibrated to percent albedo * 10, and bands 3, 4, and 5 were calibrated to K * 10. Images were resampled once as part of the georeferecing process.

The equations for snow cover and green biomass estimation were put into an Avenue script to be run in ArcView. The script prompts the user to pick band 1, 2, and 4. Once the bands are picked and $snowcover_{b4}$ runs the user is prompted to name the estimated snow cover grid. The script runs tNDVI6 and prompts the user to name the estimated green biomass grid. The snow cover equation required band 4 from a navigated and calibrated AVHRR satellite image and it contained the equation $snowcover_{b4}$. A legend file set the $snowcover_{b4}$ values to 20 classes from 0 to 100%, with a gray to red color scale that is consistent for each image. $Snowcover_{b4}$ values above 111 and below - 7 were set as NO DATA and appear the same color as the background. NO DATA might be interpreted as bare ground or cloud cover, depending on the persistence of the NO DATA pattern, since clouds are ephemeral. The 95% confidence interval, ASC, and comparison between images were used to determine these limits.

The green biomass portion of the script involved three steps. The NDVI was calculated and scaled using the equation ((NDVI + 1) / 2) * 200). The green biomass was estimated using tNDVI6. A legend file that converted the tDNVI6 value to a green color scale set the lower limit at 101, with values below 250 kg/ha coded to a blue scale and values above to a green scale. Although the values 101 - 250 kg/ha are questionable, it appeared that setting this range to NO DATA would have missed the onset of green up in Hayden Valley and along the Gardner River. As one might expect, there was overlap between low snow cover and green biomass, when the snow was melting and vegetation was greening. Rather than set these low ranges to NO DATA, it was left for the user to determine the settings specific to the application. No upper limit was set for the green biomass estimate. It appeared that setting limits for estimated snow cover and green biomass served as a cloud mask. A forest mask was included in the algorithm because the

study was conducted in non-forested habitat types. Issues of remotely sensing snow cover in forest were not addressed.

This algorithm was tested with spring snowmelt conditions. Due to the strong influence of satellite geometry and the difference in snow reflectance between morning and late afternoon spring snow, it was recommended that this algorithm be used with AVHRR overpasses of satellites east of the Park in the late afternoon (Wiscombe and Warren 1980, Dozier and Warren 1982, Elachi 1987, Dozier 1989, Lillesand and Kiefer 1994, Lipton and Ward 1997).

G. Bibliography

Baldwin, D.G., and W.J. Emery. 1993. A systematized approach to AVHRR Image Navigation. *Annals of Glaciology*. 17:414-420.

Barnes, J.C., and C.J. Bowley. 1972. *Snow studies using thermal infrared measurements from Earth satellites*. Department of Commerce National Oceanic and Atmospheric Administration National Environmental Satellite Service. Hammonds Ferry Road, Baltimore, Maryland.

Basist, A., D. Garrett, R. Ferraro, N. Grody, and K. Mitchell. 1996. A comparison between snow cover products derived from visible and microwave satellite observations. *Journal of Applied Meteorology*. pp.163-177.

Box, E.O., B.N Holben, and V. Kalb. 1989. Accuracy of the AVHRR vegetation index as a predictor of biomass, primary productivity and net CO_2 flux. *Vegetatio*. 80:71-89.

Carroll, T.R. 1990. Operational airborne and satellite snow cover products of the National Operational Hydrologic Remote Sensing Center. *Proceedings of the Forty-seventh Annual Eastern Snow Conference*. June 7-8, 1990. Bangor, Maine, CRREL Special Report 90-44.

Despain, D.G. 1990. *Yellowstone Vegetation: Consequences of environment and history in a natural setting*. Roberts Rinehart Publishers. Boulder, Colorado. (http://www.nps.gov/yell/technical/gis/download.htm)

Derrien, M., B. Farki, L. Harang, H. LeGleau, A. Noyalet, D. Pochic, and A. Sairouni. 1993. Automatic cloud detection applied to NOAA-11/AVHRR imagery. *Remote Sensing of Environment*. 46:246-267.

Dozier, J., and S.G. Warren. 1982. Effect of viewing angle on the infrared brightness temperature of snow. *Water Resources Research*. 18:1424-1434.

Dozier, J. 1989. Spectral signature of alpine snow cover from the Landsat Thematic Mapper. *Remote Sensing of Environment*. 28:9-22.

Elachi, C. 1987. *Introduction to the Physics and Techniques of Remote Sensing*. John Wiley & Sons, Inc. USA.

Emery, W.J., J. Brown and V.P. Novak. 1989. AVHRR image navigation: summary and review. *Photogrammetric Engineering and Remote Sensing*. 8:1175-1183.

EROS Data Center. 1996. Readme.1st, The 1996 Conterminous U.S. AVHRR Biweekly Composites. CD-ROM. National Mapping Division U.S. Geological Survey EROS Data Center. Sioux Falls, South Dakota.

Hall, D.K., A.T.C. Chang, J.L. Foster, C.S. Benson, and W.M. Kovalick. 1989. Comparison of in situ and Landsat derived reflectance of Alaskan glaciers. *Remote Sensing Environment*. 28:23-31.

Hall, D.K., G.A. Riggs, and V.V. Salomonson. 1995. Development of methods for mapping global snow cover using moderate resolution imaging spectroradiometer data. *Remote Sensing of Environment*. 54:127-140.

Hanson, D. 2000. Using advanced very high resolution radiometer (AVHRR) satellite images to map snow cover and green biomass in Yellowstone National Park. M.S. Thesis. Montana State University-Bozeman. Bozeman, Montana.

Hastings, D.A., and W.J. Emery. 1992. The advanced very high resolution radiometer (AVHRR): a brief reference guide. *Photogrammetric Engineering and Remote Sensing*. 58:1183-1188.

Hobbs, N.T., D.L. Baker, J.E. Ellis, and D.M. Swift. 1981. Composition and quality of elk winter diets in Colorado. *Journal of Wildlife Management*. 45:156-171.

Holben, B.N. 1986. Characteristics of maximum-value composite images from temporal AVHRR data. *International Journal of Remote Sensing*. 7:1417-1434.

Holroyd, E.W. III, J.P. Verdin, and T.R. Carroll. 1989. Mapping snow cover with satellite imagery: comparison of results from three sensor systems. *Proceedings of the fifty-seventh Western Snow Conference*. Fort Collins, Colorado.

Holroyd, E.W. III, and T.R. Carroll. 1990. Further refinements in the remote sensing of snow-covered areas. Presented at the American Society of Photogrammetry and Remote Sensing Annual Meeting. Denver, Colorado. March 1990.

Huete, A.R., and C.J. Tucker. 1991. Investigation of soil influences in AVHRR red and near-infrared vegetation index imagery. *International Journal of Remote Sensing*. 12:1223-1242

Jensen, J.R. 1996. *Introductory Digital Image Processing: A remote sensing perspective*. Second ed. Prentice Hall, Upper Saddle River, New Jersey.

Jin, Z., and J.J. Simpson. 1999. Bidirectional anisotropic reflectance of snow and sea ice in AVHRR channel 1 and 2 spectral regions - Part I: Theoretical analysis. *IEEE Transactions on Geoscience and Remote Sensing*. 37:543-554.

Justice, C.O., and P.H. Hiernaux. 1986. Monitoring the grasslands of the Sahel using NOAA AVHRR data: Niger 1983. *International Journal of Remote Sensing*. 7:1475-1497.

Justice, C.O., J.R. Townshend, B.N. Holben, and C.J. Tucker. 1985. Analysis of the phenology of global vegetation using meteorological satellite data. *International Journal of Remote Sensing*. 6:1271-1318.

Kennedy, P. 1989. Monitoring the vegetation of Tunisian grazing lands using the normalized difference vegetation index. *Ambio*. 18:119-123.

Kidwell, K.B. 1991. *NOAA Polar Orbiter data users guide: TIROS-N, NOAA-6, NOAA-7, NOAA-8, NOAA-9, NOAA-10, NOAA-11, and NOAA-12.* NOAA/NESDIS/NCDC/SDSD. Washington, D.C.

Lawrence, R.L., and W.J. Ripple. 1998. Comparisons among vegetation indices and bandwise regression in a highly disturbed, heterogeneous landscape: Mount St. Helens, Washington. *Remote Sensing of Environment.* 64:91-102.

Lillesand, T.M., and R.W. Kiefer. 1994. *Remote Sensing and Image Interpretation.* John Wiley & Sons, Inc. New York, New York.

Lindsay, R., and D. Rothrock. 1993. The calculation of surface temperature and albedo of Arctic sea ice from AVHRR. *Annals of Glaciology.* 17:391-397.

Lipton, A.E., and J.M. Ward. 1997. Satellite-view biases in retrieved surface temperatures in mountain areas. *Remote Sensing of Environment.* 60:92-100.

Navigate ReadMe. Undated. Navigation software. Nav.doc.ascii. Department of Aerospace Engineering Sciences, University of Colorado. Boulder, Colorado.

Planet, W.G., ed. 1988. *Data extraction and calibration of Tiros-N/NOAA radiometers, NOAA Technical Memorandum NESS 107 - Rev. 1.* U.S. Department of Commerce, NOAA/NESDIS. Washington D.C.

Rosborough, G.W., D.G., Baldwin, and W.J. Emery. 1994. Precise AVHRR image navigation. *IEEE Geoscience and Remote Sensing.* 32:644-657.
Sabins, F.F. 1996. *Remote sensing: Principles and interpretations.* Third edition.W.H. Freeman and Company. New York, New York.

Salisbury, J.W., D.M. D'Aria, and A.E. Wald. 1994. Measurements of thermal infrared spectral reflectance of frost, snow, and ice. *Journal of Geophysical Research.* 99:24235-24240.

Skidmore, P., K. Hansen, and W. Quimby. 1994. Snow accumulation and ablation under fire-altered lodgepole pine forest canopies. Abstracts of the Western Snow Conference. Santa Fe, New Mexico.

Thoma, D.P. 1998. *Near real-time satellite and ground based radiometric estimation of vegetation biomass, and nitrogen content in Montana rangelands.* M.S. Thesis. Montana State University-Bozeman. Bozeman, Montana.

Wald, A.E. 1994. Modeling thermal infrared (2-14 μm) reflectance spectra of frost and snow. *Journal of Geophysical Research.* 99:24235-24240.

Wiscombe, W.J. and S.G. Warren. 1980. A model for the spectral albedo of snow. I: Pure snow. *Journal of the Atmospheric Sciences.* 37:2712-2733.

Yellowstone National Park. Online material.
http://www.nps.gov/yell/gis/dem30m.html.

APPENDIX B

GROUND CONTROL POINTS ON AN IMAGE

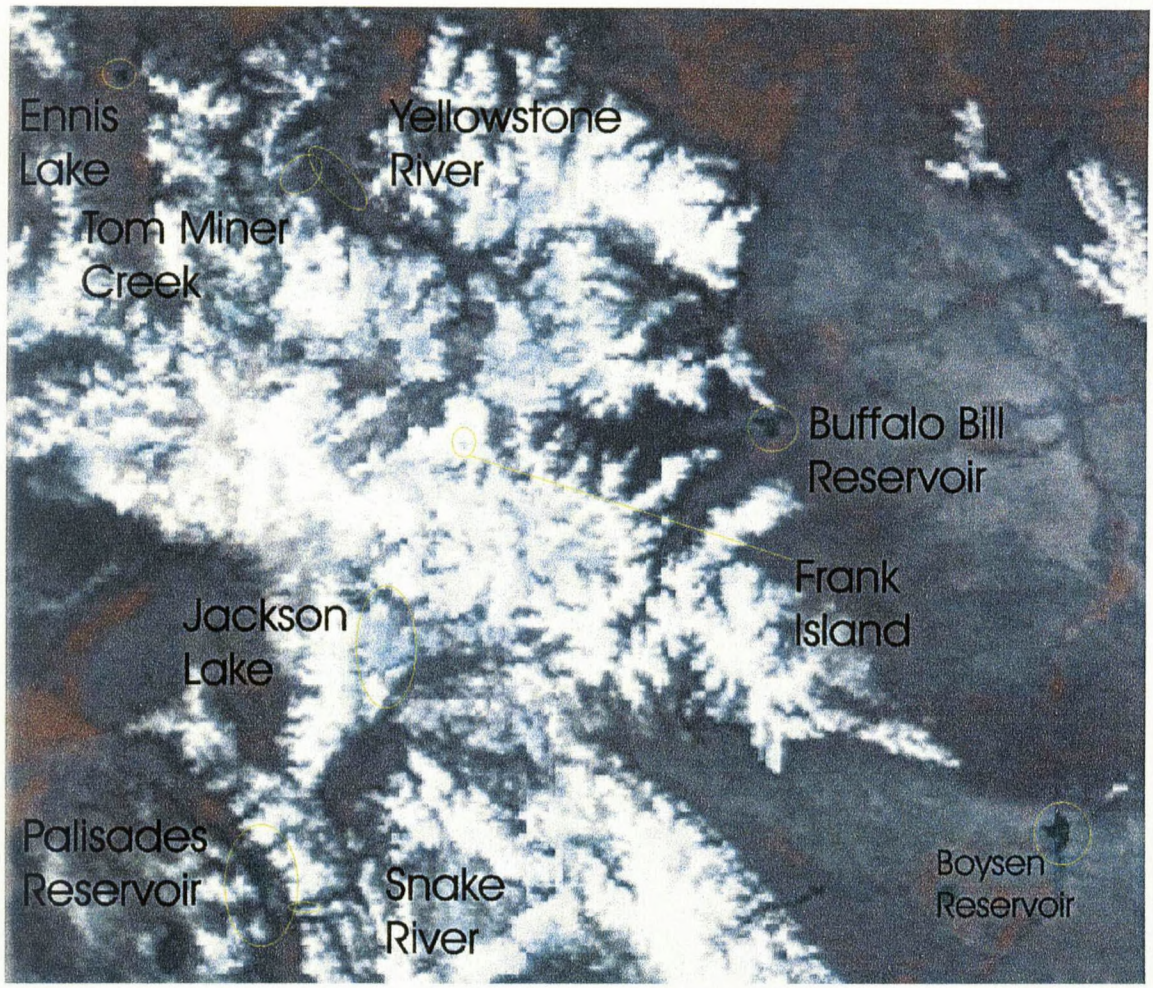
Ennis
Lake
Yellowstone
River
Tom Miner
Creek
Buffalo Bill
Reservoir
Frank
Island
Jackson
Lake
Palisades
Reservoir
Snake
River
Boysen
Reservoir

APPENDIX C

AVENUE SCRIPT

```
theTitle = "Snow and Veg Model: AVHRR"

'Set the Work Directory, Project, get Active View and set Projection
theProject = av.GetProject
theWorkDir = theProject.GetWorkDir
theWorkDir.SetCWD
theView = av.GetActiveDoc
thePrj = theView.GetProjection

' Equations as strings for output
SnowcovEqn = "(1261.7543 - (band4 * 0.4282))"
SnowCovUnits = "units are % snow cover"
GrnbioEqn = "ScaledNDVI = ((((band2-band1)/(band2+band1))+1)/2)*200"
GreenBioEqn = "-2860.9+(25.8*Scaled NDVI)"
GreenBioUnits = "units are kg/ha"


' ------------------------------------------------------------------
' Create a List of GRID Themes in the View
theView = av.GetActiveDoc
ThemeList = List.Make
for each t in theView.GetThemes
  if (t.Is(GTHEME)) then
    ThemeList.Add(t)
  end
end

' ------------------------------------------------------------------
' Select the Bands 1,2,4 Themes

bTheme = MsgBox.List(ThemeList, "Pick Band 1", theTitle ++ "Band 1")
if (bTheme = nil) then
  return nil
else
  band1 = bTheme.getgrid
end
ThemeList.RemoveObj(bTheme)
bTheme = MsgBox.List(ThemeList, "Pick Band 2", theTitle)
band2 = bTheme.getgrid
b2Name = bTheme.GetName
b2Comments = bTheme.GetComments

ThemeList.RemoveObj(bTheme)
bTheme = MsgBox.List(ThemeList, "Pick Band 4", theTitle)
band4 = bTheme.getgrid
b4Name = bTheme.GetName
b4Comments = bTheme.GetComments
ThemeList.RemoveObj(bTheme)

Snowcovb4 = (1261.7543.AsGrid - (band4 * 0.4282.AsGrid))

grnbio = (((((band2.float - band1.float)/(band2.float + band1.float))
      + 1.AsGrid) / 2.AsGrid)) * 200.AsGrid
greenbio = -2860.9.AsGrid + (25.8.AsGrid * grnbio.float)

' SnowModel 1
theGTheme1 = GTheme.Make(Snowcovb4)                ' Create a Theme
theGTheme1.SetName("Snowcovb4:" ++ b4Name)         ' Set Name of Theme
theView.AddTheme(theGTheme1)                       ' Add Theme to the
View
```

```
Message = "Snowcovb4: " ++ b4Name + nl + SnowCovUnits + nl + SnowcovEqn
      + nl + b4Comments
theGTheme1.SetComments(Message)

' Save the Grid if required
' Get output filename to save the model output as a file
def = Snowcovb4.GetSrcName.GetFileName
aFN = SourceManager.PutDataSet(GRID,"Save Data Set:
      " + Snowcovb4.GetName,def,FALSE)
if (aFN = NIL) then
  return(nil)
end'

' Save to permanent file name
status = Grid.GetVerify
Grid.SetVerify(#GRID_VERIFY_OFF)
if (Snowcovb4.SaveDataSet(aFN).Not) then
      Grid.SetVerify(status)
end
Grid.SetVerify(status)

' GreenBiomassModel 1
theGTheme2 = GTheme.Make(greenbio)                    ' Create a Theme
theGTheme2.SetName("greenbio:" ++ b2Name )            ' Set Name of Theme
theView.AddTheme(theGTheme2)                          ' Add Theme to the
View
Message = "GreenBio:" ++ b2Name + nl + GreenBioUnits + nl + GrnbioEqn +
      nl + GreenBioEqn + nl + b2Comments
theGTheme2.SetComments(Message)

' Save the Grids if required
' Get output filename to save the model output as a file
def = greenbio.GetSrcName.GetFileName
aFN = SourceManager.PutDataSet(GRID,"Save Data Set:
      " + Greenbio.GetName,def,FALSE)
if (aFN = NIL) then
  return(nil)
end'

' Save to permanent file name
status = Grid.GetVerify
Grid.SetVerify(#GRID_VERIFY_OFF)
if (greenbio.SaveDataSet(aFN).Not) then
   Grid.SetVerify(status)
end
Grid.SetVerify(status)
```